# Interphase effect on the controlled frequency response of three-phase smart magneto-electro-elastic plates embedded with active constrained layer damping: FE study

To cite this article: M Vinyas 2019 *Mater. Res. Express* **6** 125707



Materials Research Express

RECEIVED
9 September 2019

REVISED
10 December 2019

ACCEPTED FOR PUBLICATION
30 December 2019

PUBLISHED
10 January 2020

PAPER

# Interphase effect on the controlled frequency response of three-phase smart magneto-electro-elastic plates embedded with active constrained layer damping: FE study

**M Vinyas**

Non-linear Multifunctional Composites Analysis and Design (NMCAD) lab, Department of Aerospace Engineering, Indian Institute of Science, Bangalore-560012, India

**E-mail:** vinyasmahesh@iisc.ac.in **and** Vinyas.mahesh@gmail.com

**Keywords:** interphase, coupling, magneto-electro-elastic, finite elements, active constrained layer damping

## Abstract

In this article, the controlled frequency response of three-phase smart magneto-electro-elastic (TPS-MEE) composite plates treated with active constrained layer damping (ACLD) is studied using finite element (FE) method. The composite consists of Cobalt Ferrite piezomagnetic matrix embedded with carbon fibers in the piezoelectric shell. A three-dimensional FEformulation is developed through the principle of virtual work. The ACLD treatment comprises of the constraining layer of 1–3 piezoelectric composite as well as the constrained layer of viscoelastic material. The coupling characteristics and hence the stiffness of the smart composite significantly change with the thickness of the piezoelectric interphase. Therefore, emphasis is made on the effect of ACLD treatment on the vibration attenuation of the TPS-MEE plates with different interphase thickness and material. In addition, special attention is paid to the influence of geometrical skewness associated with different interphase thickness on the vibration amplitude and the control voltage.

## 1. Introduction

Among the many available smart materials, magneto-electro-elastic (MEE) materials have proved to be a potential candidate for many engineering applications due to its inherent coupling capabilities. This material is comprised of piezoelectric and piezomagnetic phases and exhibits a superior magnetoelectric (ME) coupling which is not observed in the individual phases [1, 2]. Boomgard and Born [3] for the first time attempted to fabricate the ME composites using Barium Titanate ($BaTiO_3$) and Nickel Ferrite ($NiFe_2O_4$) through sintering technique. Boomgard *et al* [2] found that the ME properties of MEE materials are significantly affected by the combined phases of Barium Titanate ($BaTiO_3$) –Cobalt Ferrite ($CoFe_2O_4$) present in the composite. Many researchers have attempted to study the material properties of MEE composites incorporating numerous computational methods such as micromechanical approaches [4–6] (e.g. asymptotic homogenization method [7–9], self-consistent method [10, 11], and Mori-Tanaka method [12–14]). Shen and Li [15], Sevastionav and Kachanov [16] and Aboudi [17] adopted the homogenization technique to the estimation of the coupled effective material coefficients of magneto-electro-thermo-elastic (METE)materials. That the inhomogeneity associated with the microstructure of METE material affects the effective material constants was thoroughly studied by Koutsawa *et al* [18–20]. The influence of multi-inclusions and arbitrary lamination on the coupled characteristics of MEE material was investigated by Li [21] and Giordano *et al* [22], respectively. Lee *et al* [23] incorporated finite element (FE) methods to determine the MEE material properties. Tang and Yu [24–26] and Yu and Tang [27, 28] adopted variational asymptotic methods for unit cell homogenisation (VAMUCH) to predict the local fields of METE materials. Similarly, asymptotic homogenization scheme [29–32] is also found to be effective in predicting the characteristics properties of METE materials.

Alongside, a plenty of attempts have been made by the researchers to explore the mechanical response of MEE structures incorporating different computational techniques. Through exact solutions, Pan and co-workers [33, 34]

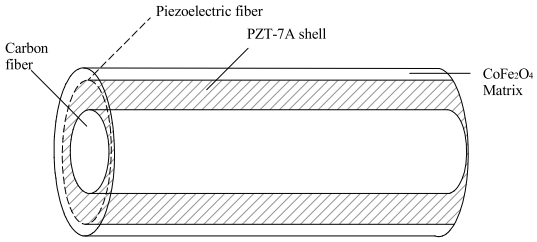


(a) piezoelectric fiber distributed in piezomagnetic matrix

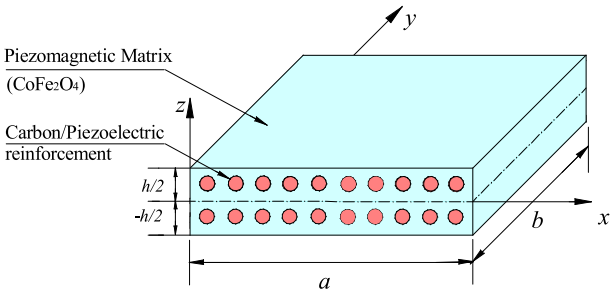


(b) TPS-MEE plate

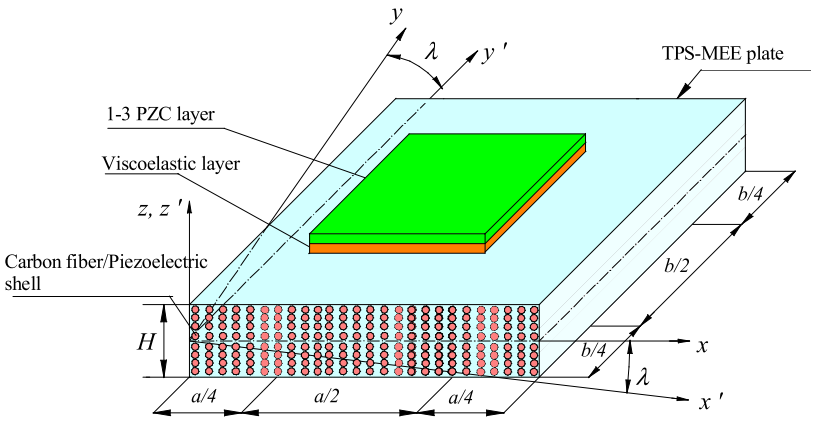


(c) ACLD treated skew TPS-MEE plate

**Figure 1.** Schematic representation of smart carbon-piezoelectric fiber (b) TPS-MEE plate geometry (c) ACLD treated TPS-MEE skew plate.

evaluated the natural frequencies of MEE multilayered plates. Lage *et al* [35] adopted partial FE methods to probe the mechanical behaviour of MEE plates. Vinyas [36] made use of FE methods to assess the coupled response of carbon nano tube reinforced MEE plates. In addition, other computational techniques, such as state space approach [37–41], approximation technique [42, 43], FE methods [44–48], semi-analytical FE method [49], meshless technique [50] have also been proved the credibility in determining the frequency response of MEE structures. In addition, static response of MEE structures under various working environment has also been reported [51–61].

A structure in practical operation usually is subjected to hazardous vibrations which deteriorate its performance. In addition, it may also reduce the service life of the structure due to resonance. One of the solutions that the researchers have effectively found out to attenuate the unwanted vibrations is through the active constrained layer damping (ACLD) treatment. In this technique the constraining layer of 1–3 piezoelectric composite (PZC) patch and the constrained layer low stiff viscoelastic material are both used. Previous studies have highlighted that in contrast to the monolithic piezoelectric patch, superior damping properties are exhibited by the piezoelectric fiber reinforced epoxy matrix (i.e. the 1–3 PZC) [62] as a constrained layer. The credibility of adopting ACLD treatment is demonstrated in various research works. Ray and Pradhan [63] probed the damped frequency characteristics of composite plates through FE methods. In addition, Ray and co-workers assessed the attenuation response of functionally graded [64–66], laminated [67–69] and sandwich [70, 71] plates with ACLD treatment. The effect of ACLD patch on the damping behaviour of skew plates was

**Table 1.** Material properties of TPS-MEE material with different interphase thickness and volume fraction [82–84].

| Material property | Material constant | $\delta$ | PZT-5A | | | | PZT-7A | | | |
|---|---|---|---|---|---|---|---|---|---|---|
| | | | $V_f = 0.2$ | $V_f = 0.3$ | $V_f = 0.4$ | $V_f = 0.5$ | $V_f = 0.2$ | $V_f = 0.3$ | $V_f = 0.4$ | $V_f = 0.5$ |
| Elastic | $C_{11} = C_{22}$ | 0.36 | 204.53 | 177.69 | 155.43 | 137.76 | 222.37 | 199.21 | 178.89 | 161.39 |
| Constant | | 0.25 | 191.93 | 162.23 | 139.4 | 120.58 | 208.93 | 180.83 | 159.8 | 143 |
| (Gpa) | | 0.13 | 173.61 | 143.34 | 117.65 | 100.54 | 184.19 | 153.96 | 131.51 | 112.6 |
| | | 0.01 | 144.98 | 118.85 | 88.45 | 69.63 | 146 | 112.24 | 89.79 | 73 |
| | $C_{12}$ | 0.36 | 121.15 | 104.7 | 91.54 | 81.03 | 128.78 | 113.38 | 101.21 | 91.06 |
| | | 0.25 | 111.91 | 94.14 | 80.33 | 69.48 | 119.89 | 102.06 | 88.68 | 78.12 |
| | | 0.13 | 98.72 | 78.96 | 65.81 | 55.29 | 103.73 | 84.69 | 70.9 | 59.13 |
| | | 0.01 | 77.27 | 57.19 | 43.38 | 34.18 | 77.07 | 56 | 43.83 | 33.68 |
| | $C_{13} = C_{23}$ | 0.36 | 122.11 | 106.78 | 93.64 | 83.61 | 127.51 | 111.86 | 98.76 | 88.22 |
| | | 0.25 | 111.13 | 92.98 | 79.21 | 67.96 | 116.56 | 98.35 | 83.79 | 72.52 |
| | | 0.13 | 93.56 | 73.84 | 59.13 | 49.45 | 97.57 | 77.9 | 62.25 | 51.34 |
| | | 0.01 | 64.39 | 43.09 | 29.01 | 19.64 | 63.98 | 42.49 | 28.66 | 19.94 |
| | $C_{44} = C_{55}$ | 0.36 | 41.83 | 40.21 | 38.5 | 36.88 | 43.21 | 42.27 | 41.24 | 40.21 |
| | | 0.25 | 41.39 | 39.85 | 38.14 | 36.52 | 42.6 | 41.37 | 40.14 | 39 |
| | | 0.13 | 41.21 | 39.41 | 37.61 | 35.99 | 41.9 | 40.36 | 38.93 | 37.39 |
| | | 0.01 | 40.67 | 38.87 | 37.25 | 35.18 | 40.99 | 39.26 | 37.32 | 35.58 |
| Piezoelectric | $e_{31}$ | 0.36 | −1.25 | −1.69 | −2.02 | −2.29 | −1.31 | −1.94 | −2.16 | −2.42 |
| Constants | | 0.25 | −1.02 | −1.33 | −1.56 | −1.75 | −1.11 | −1.45 | −1.89 | −1.86 |
| | | 0.13 | −0.64 | −0.79 | −0.92 | −1.01 | −0.79 | −0.89 | −0.99 | −1.16 |
| | | 0.01 | −0.001 | −0.021 | −0.027 | −0.075 | −0.012 | −0.027 | −0.032 | −0.095 |
| | $e_{33}$ | 0.36 | 1.377 | 2.274 | 3.171 | 4.144 | 1.402 | 2.473 | 3.296 | 4.349 |
| | | 0.25 | 0.909 | 1.579 | 2.223 | 2.969 | 1.02 | 1.978 | 2.789 | 3.165 |
| | | 0.13 | 0.871 | 1.579 | 2.223 | 2.994 | 0.923 | 1.697 | 2.453 | 3.102 |
| | | 0.01 | 0.0379 | 0.0631 | 0.0961 | 0.1024 | 0.0497 | 0.0983 | 0.1631 | 0.1098 |
| | $e_{15}$ | 0.36 | 0.035 21 | 0.059 72 | 0.089 27 | 0.131 39 | 0.051 093 | 0.088 562 | 0.136 415 | 0.202 93 |
| | | 0.25 | 0.034 58 | 0.057 84 | 0.088 | 0.130 77 | 0.051 086 | 0.089 606 | 0.137 45 | 0.200 85 |
| | | 0.13 | 0.031 43 | 0.052 81 | 0.083 61 | 0.122 59 | 0.051 09 | 0.082 342 | 0.126 03 | 0.1853 |
| Dielectric | | 0.01 | 0.0044 | 0.005 66 | 0.008 17 | 0.010 69 | 0.004 408 | 0.005 579 | 0.008 815 | 0.009 99 |
| Constants | $\eta_{11} = \eta_{22}$ | 0.36 | 0.1209 | 0.149 64 | 0.182 753 | 0.232 668 | 0.121 | 0.147 068 | 0.187 01 | 0.2369 |
| ($10^{-9}$ C$^2$ N$^{-1}$m$^{-2}$) | | 0.25 | 0.1132 | 0.139 06 | 0.176 43 | 0.2263 | 0.117 614 | 0.146 179 | 0.182 755 | 0.23 |
| | | 0.13 | 0.1132 | 0.139 06 | 0.176 43 | 0.2263 | 0.118 501 | 0.142 627 | 0.173 86 | 0.2184 |
| | | 0.01 | 0.085 33 | 0.091 94 | 0.095 67 | 0.102 28 | 0.087 376 | 0.092 821 | 0.095 59 | 0.1001 |
| | $\eta_{33}$ | 0.36 | 1.9039 | 2.788 | 3.687 | 4.572 | 2.01 | 2.97 | 3.89 | 5.03 |

**Table 1.** (Continued.)

| Material property | Material constant | $\delta$ | PZT-5A | | | | PZT-7A | | | |
|---|---|---|---|---|---|---|---|---|---|---|
| | | | $V_f = 0.2$ | $V_f = 0.3$ | $V_f = 0.4$ | $V_f = 0.5$ | $V_f = 0.2$ | $V_f = 0.3$ | $V_f = 0.4$ | $V_f = 0.5$ |
| | | 0.25 | 1.3953 | 2.0795 | 2.737 | 3.394 | 1.4535 | 2.123 | 2.945 | 3.546 |
| | | 0.13 | 0.8331 | 1.2095 | 1.545 | 1.9491 | 0.899 | 1.278 | 1.601 | 2.456 |
| Magnetic | | 0.01 | 0.1103 | 0.112 | 0.1137 | 0.1288 | 0.1109 | 0.1132 | 0.1149 | 0.1301 |
| Permeability | $\mu_{11} = \mu_{22}$ | 0.36 | −3.845 | −3.0829 | −2.4076 | −1.873 66 | −3.856 55 | −3.070 69 | −2.430 35 | −1.848 23 |
| ($10^{-4}$Ns$^2$/C$^2$) | | 0.25 | −3.8432 | −3.0825 | −2.4072 | −1.8734 | −3.856 51 | −3.070 63 | −2.430 31 | −1.848 21 |
| | | 0.13 | −3.8429 | −3.0821 | −2.4068 | −1.8729 | −3.856 48 | −3.070 59 | −2.430 28 | −1.848 18 |
| | | 0.01 | −3.8425 | −3.0819 | −2.4065 | −1.8725 | −3.856 45 | −3.070 55 | −2.430 26 | −1.848 15 |
| | $\mu_{33}$ | 0.36 | 1.265 | 1.111 46 | 0.961 618 | 0.811 78 | 1.267 26 | 1.113 92 | 0.969 258 | 0.818 806 |
| | | 0.25 | 1.2642 | 1.111 41 | 0.961 611 | 0.811 73 | 1.267 21 | 1.113 86 | 0.969 251 | 0.8188 |
| | | 0.13 | 1.2633 | 1.111 37 | 0.961 608 | 0.811 69 | 1.267 18 | 0.113 83 | 0.959 245 | 0.8183 |
| Piezomagnetic | | 0.01 | 1.2621 | 1.111 31 | 0.961 602 | 0.811 65 | 1.267 15 | 0.113 79 | 0.959 24 | 0.8181 |
| Constants | $q_{31}$ | 0.36 | 345.34 | 267.03 | 206.37 | 157.47 | 367.99 | 301.48 | 238.56 | 188.76 |
| (N/Am) | | 0.25 | 326.71 | 251.34 | 189.7 | 140.8 | 345.34 | 268.03 | 203.37 | 156.47 |
| | | 0.13 | 300.24 | 223.89 | 165.19 | 123.16 | 326.71 | 250.34 | 190.7 | 141.08 |
| | | 0.01 | 257.1 | 184.68 | 133.82 | 97.66 | 300.24 | 221.89 | 167.19 | 124.2 |
| | $q_{33}$ | 0.36 | 478.24 | 395.55 | 322.49 | 256.31 | 488.181 | 401.28 | 328.62 | 262.3 |
| | | 0.25 | 449.36 | 365.3 | 292.24 | 231.56 | 461.25 | 377.52 | 301.69 | 240.13 |
| | | 0.13 | 417.73 | 329.54 | 261.98 | 204.05 | 421.66 | 336.34 | 306.86 | 208.46 |
| | | 0.01 | 359.97 | 274.53 | 212.47 | 162.79 | 362.89 | 278.57 | 213.01 | 163.53 |
| | $q_{15}$ | 0.36 | 360.01 | 283.69 | 225.85 | 169.99 | 371.4 | 294.98 | 233.58 | 179.69 |
| | | 0.25 | 336.4 | 267.54 | 200.69 | 152.36 | 348.87 | 272.45 | 209.55 | 160.16 |
| | | 0.13 | 305.9 | 229.63 | 172.63 | 125.21 | 314.32 | 237.9 | 179.5 | 133.12 |
| | | 0.01 | 253.74 | 183.93 | 130.12 | 94.7 | 255.74 | 186.82 | 134.44 | 97.07 |
| Magneto-Electric | $m_{11} = m_{22}$ | 0.36 | 1.7843 | 2.3254 | 2.8053 | 3.1708 | 1.801 | 2.35 | 2.95 | 3.29 |
| Constant | | 0.25 | 1.1431 | 1.4704 | 1.7748 | 2.010 52 | 1.163 | 1.501 | 1.794 | 2.02 |
| ($10^{-12}$ Ns V$^{-1}$C$^{-1}$) | | 0.13 | 0.54 | 0.6918 | 0.8129 | 0.9036 | 0.65 | 0.73 | 0.836 | 0.95 |
| | | 0.01 | 0.1507 | 0.1698 | 0.1717 | 0.1754 | 0.161 | 0.17 | 0.1729 | 0.1769 |
| | $m_{33}$ | 0.36 | 1.3495 | 1.628 | 1.7014 | 1.79 | 1.41 | 1.701 | 1.746 | 1.81 |
| | | 0.25 | 0.8161 | 0.9842 | 1.0157 | 1.0495 | 0.8811 | 1.102 | 1.035 | 1.064 |
| | | 0.13 | 0.4199 | 0.489 | 0.5161 | 0.5976 | 0.4512 | 0.5562 | 0.671 | 0.695 |
| | | 0.01 | 0.1038 | 0.1042 | 0.1059 | 0.1102 | 0.1083 | 0.1098 | 0.1074 | 0.110 93 |

**Table 2.** Verification of the natural frequencies using present FE formulation.

| Stacking Sequence | Mode No. | Non-dimensional frequency | | |
|---|---|---|---|---|
| | | Chen *et al* [40] | Present | % Error |
| *BFB* | 1 | 1.3434 | 1.3482 | 0.356 |
| | 2 | 2.2199 | 2.2279 | 0.359 |
| | 3 | 2.2199 | 2.2279 | 0.359 |
| *FBF* | 1 | 1.4463 | 1.4346 | −0.815 |
| | 2 | 2.3602 | 2.3390 | −0.906 |
| | 3 | 2.3602 | 2.3392 | −0.897 |

% Error = (Present Value - Value reported in Chen *et al* [40]/Present Value.

**Table 3.** Non-dimensional frequency parameter for the clamped-clamped laminated composite skew plate ($a/h = 10$).

| Skew angle ($\lambda$) | Source | Antisymmetric cross-ply (0°/90°/0°/90°) | | | Antisymmetric angle-ply (45°/−45°/45°/−45°) | | | Symmetric cross-ply (90°/0°/90°/0°/90°) | | |
|---|---|---|---|---|---|---|---|---|---|---|
| | | Modes | | | Modes | | | Modes | | |
| | | 1 | 2 | 3 | 1 | 2 | 3 | 1 | 2 | 3 |
| 0° | Kanasogi and Ray [72] | 2.2990 | 3.7880 | 3.7880 | 2.2119 | 3.7339 | 3.7339 | 2.3687 | 3.5399 | 4.1122 |
| | Present | 2.2990 | 3.5913 | 3.8695 | 2.1767 | 3.5746 | 3.5139 | 2.3400 | 3.3655 | 4.2382 |
| 15° | Kanasogi and Ray [72] | 2.3809 | 3.7516 | 4.0785 | 2.3099 | 3.6997 | 4.0438 | 2.4663 | 3.6255 | 4.3418 |
| | Present | 2.3992 | 3.5560 | 4.0841 | 2.2344 | 3.5111 | 3.9290 | 2.3160 | 3.4637 | 4.2346 |
| 30° | Kanasogi and Ray [72] | 2.6666 | 3.9851 | 4.7227 | 2.6325 | 3.9549 | 5.2107 | 2.7921 | 3.9557 | 5.0220 |
| | Present | 2.4903 | 3.8967 | 4.4609 | 2.4722 | 3.5807 | 5.0199 | 2.4896 | 3.6363 | 4.7949 |
| 45° | Kanasogi and Ray [72] | 3.3015 | 4.6290 | 5.8423 | 3.3015 | 4.6290 | 5.8423 | 3.4739 | 4.7129 | 5.8789 |
| | Present | 2.7948 | 4.5102 | 5.6270 | 2.8348 | 4.5102 | 5.4970 | 2.9439 | 4.6545 | 5.4362 |

studied by Kanasogi and Ray [72]. Recently, Kattimani and Ray evaluated the benefit of incorporating ACLD treatment on controlling large amplitude vibrations of MEE plate [73–75] and shell [76]structures. In addition, Vinyas and co-researchers [77–79] probed the influence of geometrical skewness on the controlled frequency response of layered, multiphase and functionally graded MEE plates, respectively.

On the other hand, the intensification of MEEcoupling phenomenon is significantly affected by the interphase region. The interphase region is a result of a chemical reaction between the matrix material and the reinforcement phase or the reinforcements may be protectively coated [80]. This interphase region can be treated as the third phase in the MEE composite and it exhibits different properties from the reinforcements and matrix. Notable consequences of the interphases linking the matrix and reinforcement have been observed on the inclusive characterization of ME smart material [81]. However, systematic analyses on the frequency response of MEE plates considering the effect of interphase are limited [82–84].

Here, we make the first endeavor to investigate the influence of ACLD treatment of the damped vibrations of three phase smart magneto-electro-elastic (TPS-MEE) plates made of carbon fiber coated with piezoelectric material and embedded in piezomagnetic matrix. Also, emphasis has been made to evaluate the effects of interphase on the controlled linear response of TPS-MEE plate for the first time. To this end, a three-dimensional FE model is developed using the principle of virtual work. The method of condensation is applied to obtain governing equations of motion which takes the coupling factors into consideration. The viscoelastic layer of ACLD is modeled through complex modulus approach [85]. In addition, a special emphasis has been made on evaluating the effect of coupling fields associated with interphase, volume fraction and geometrical skewness on the attenuated frequencies of TPS-MEE plates.

## 2. Material properties, constitutive relations and governing equations

The three-phase smart magneto-electro-elastic (TPS-MEE) material made up of smart carbon/PZT-5A(PZT-7A)/ $CoFe_2O_4$ composites is considered for evaluation. The variation in the interphase thickness of piezoelectric material (PZT-5A/PZT-7A)(figure 1(a)) is noticed to have a significant contribution on the varied material properties of the overall TPS-MEE material. Meanwhile, when the TPS-MEE material with different interphase

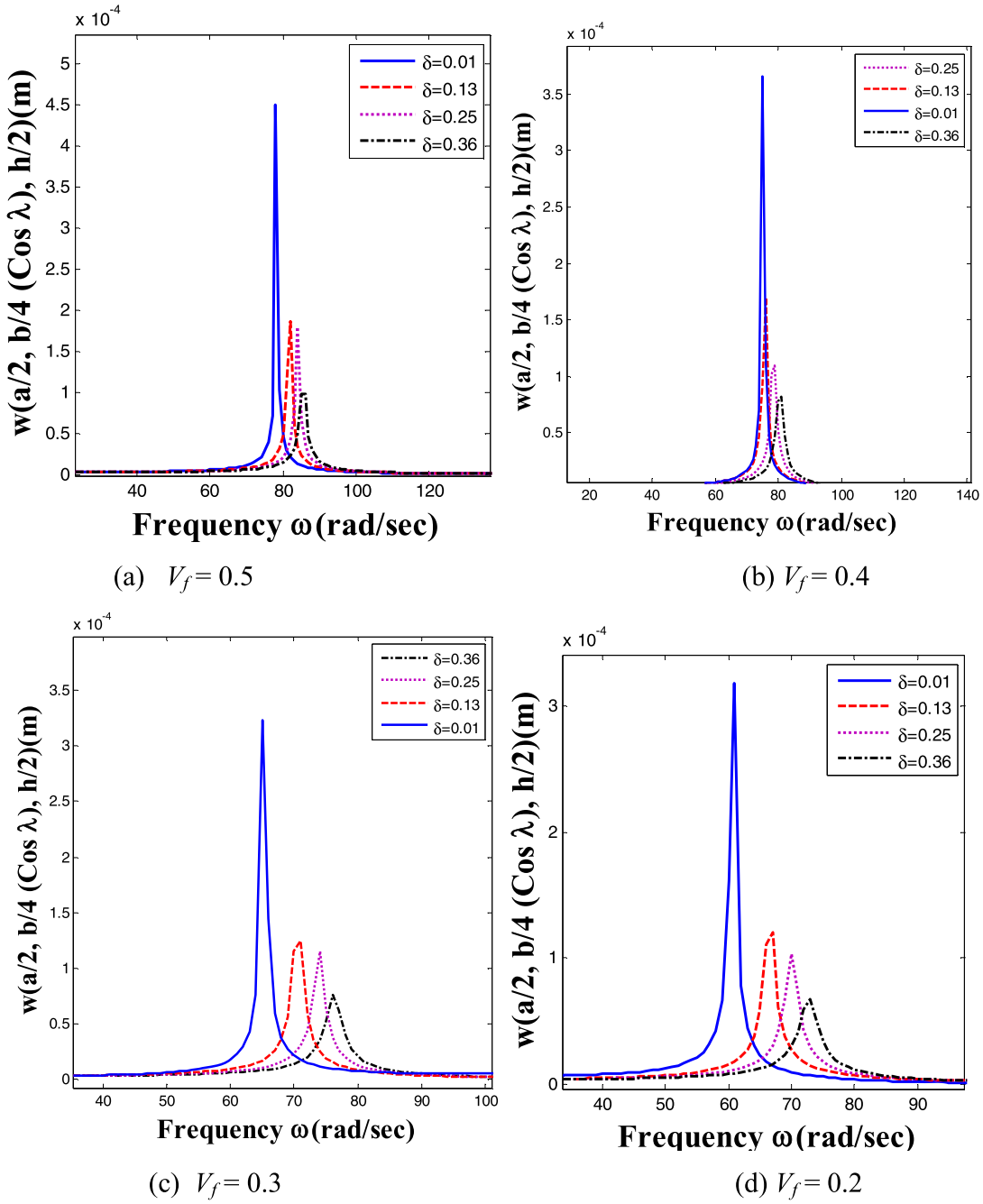


**Figure 2.** Effect of interphase thickness on the controlled linear frequency response function of deflection.

thickness is incorporated in any of the smart structures, a drastic variation in its mechanical responses is noticed. Hence, the present article aims at demonstrating the controlled frequency response of TPS-MEE plates (figure 1(b)) embedded with ACLD treatment. The material properties corresponding to the different volume fraction and interphase thickness of TPS-MEE material is tabulated in table 1.

The constitutive equations of TPS-MEE material with various interphase thickness can be expressed as follows:

$$\{\sigma^{Vf}_{b\_in}\} = [\bar{C}^{Vf}_{b\_in}]\{\varepsilon^{Vf}_{b\_in}\} - \{e^{Vf}_{b\_in}\}E_z - \{q^{Vf}_{b\_in}\}H_z;\ \{\sigma^{Vf}_{s\_in}\} = [\bar{C}^{Vf}_{s\_in}]\{\varepsilon^{Vf}_{s\_in}\} \quad (1)$$

$$D_z = \{e^{Vf}_{b\_in}\}^T\{\varepsilon^{Vf}_{b\_in}\} + \in^{Vf}_{33\_in} E_z + d_{33\_in}H_z \quad (2)$$

$$B_z = \{q^{Vf}_{b\_in}\}^T\{\varepsilon^{Vf}_{b\_in}\} + d_{33\_in}E_z + \mu_{33\_in}H_z \quad (3)$$

in which, '*Vf*' and '*in*' denotes the volume fraction and interphase thickness of TPS-MEE material. Also, $[\bar{C}^{Vf}_{b\_in}]$, $[\bar{C}^{Vf}_{s\_in}]$ relates to the elastic stiffness coefficients. The piezoelectric coefficient, the magnetostrictive coefficient

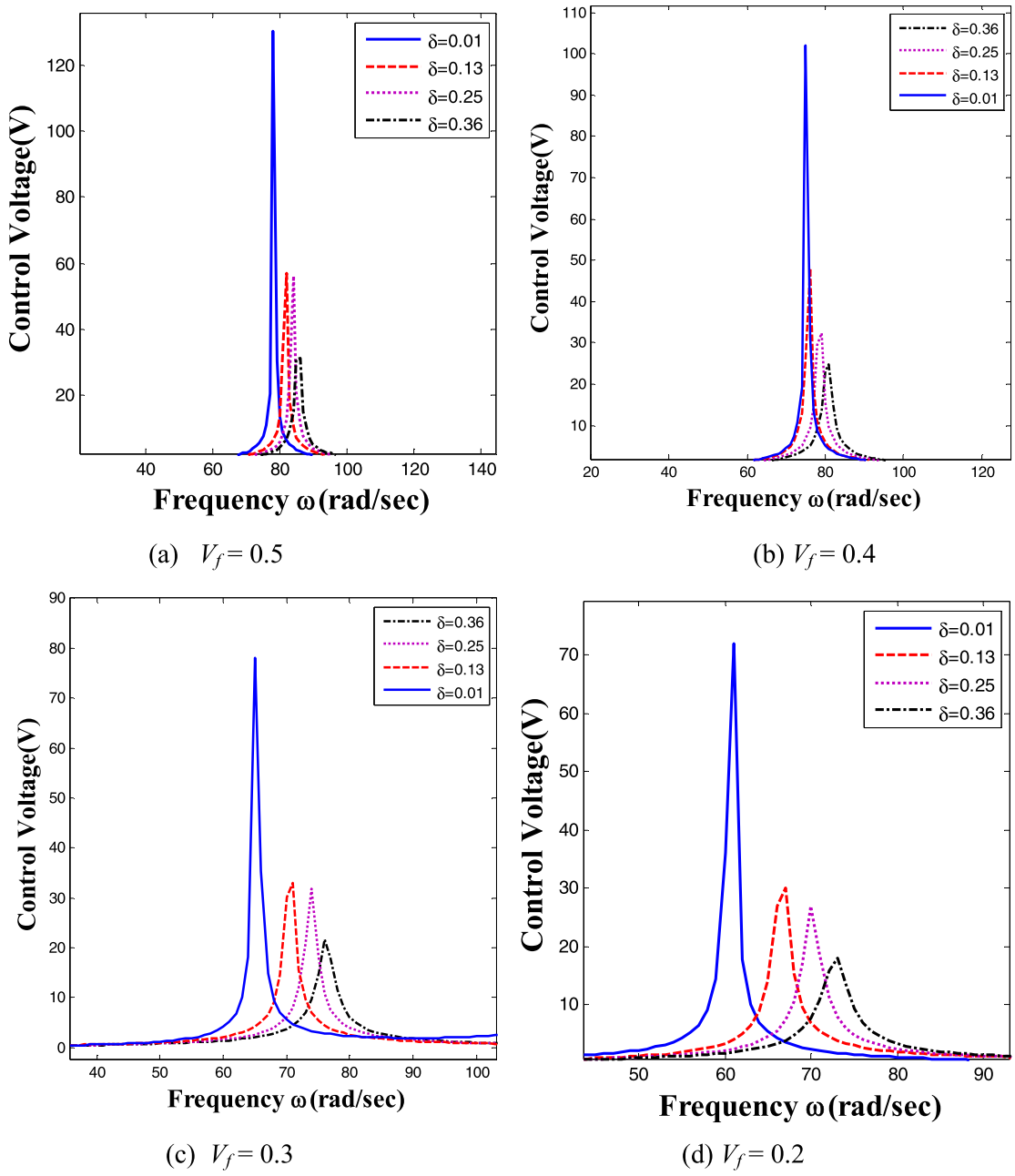


**Figure 3.** Effect of interphase thickness on the controlled linear frequency response function of control voltage.

matrices, the dielectric and electromagnetic coefficient are denoted by $\{e_{b\_in}^{Vf}\}$, $\{q_{b\_in}^{Vf}\}$, $\in_{33\_in}^{Vf}$ and $d_{33\_in}^{Vf}$, respectively. The electric displacement and magnetic flux density components of TPS-MEE material are represented by $D_z$ and $B_z$, respectively; Similarly, $E_z$ and $H_z$ are the transverse electrical field component and the magnetic field component, respectively which can be expressed with the aid of Maxwell's electromagnetic equations as follows:

$$E_z = -\frac{\partial \phi}{\partial z};\ H_z = -\frac{\partial \psi}{\partial z} \tag{4}$$

where, $\phi$ and $\psi$ are the electric and magnetic potential functions that can be represented as,

$$\phi = \frac{z - h_1}{H}\bar{\phi};\ \psi = \frac{z - h_1}{H}\bar{\psi} \tag{5}$$

The viscoelastic constrained layer of ACLD is modelled through the complex modulus approach (CMA) as follows [85]:

$$G = G'(1 + i\eta);\ E = 2G(1 + \nu) \tag{6}$$

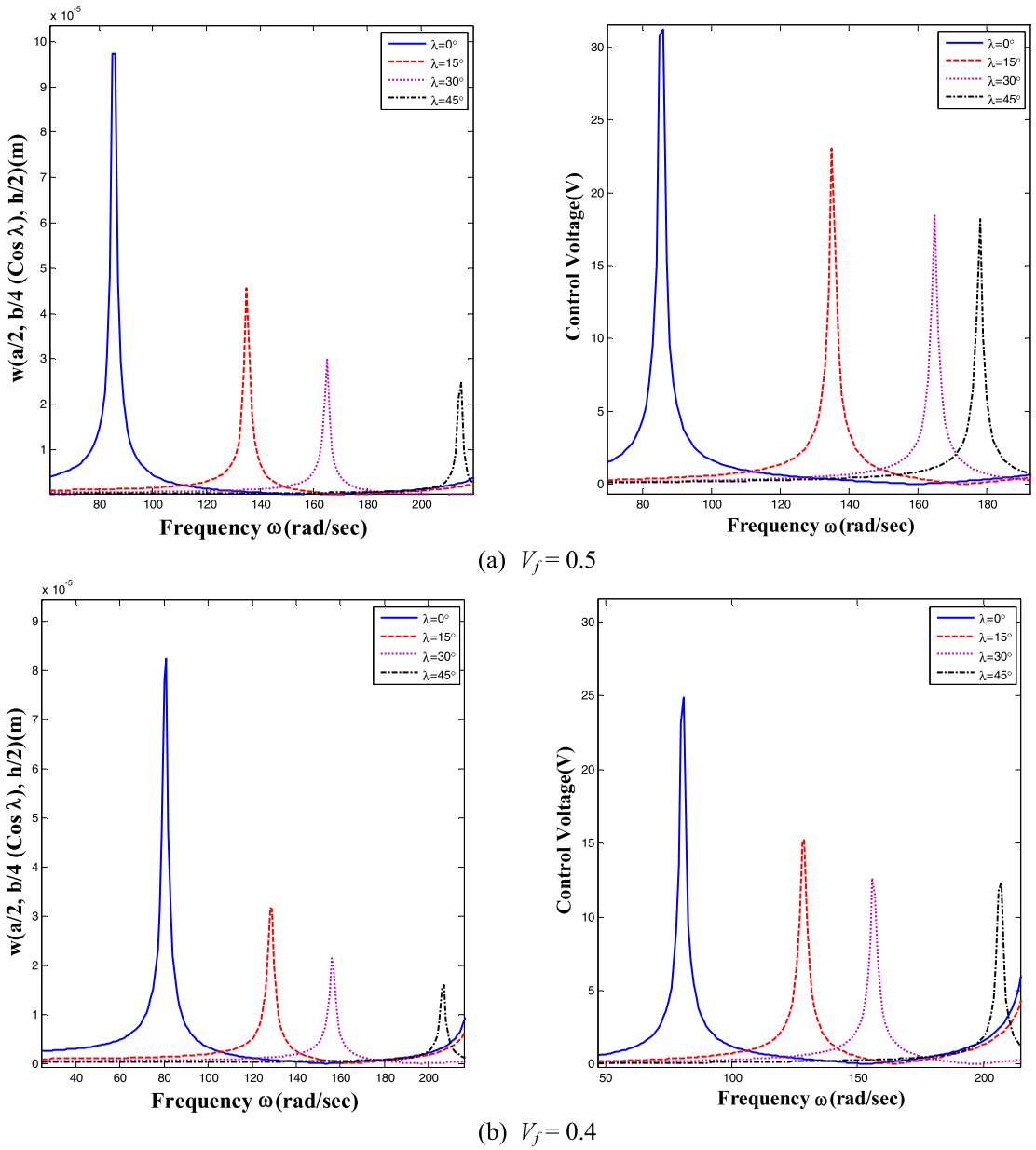


**Figure 4.** Effect of skew angle on the controlled linear frequency response function of deflection and control voltage of TPS-MEE plate ($\delta = 0.36$; PZT-7A).

where, $G'$, $\nu$ and $\eta$ corresponds to the storage modulus, Poisson's ratio and loss factor of the viscoelastic layer, respectively.

The axial displacement components $u$ and $v$ of the TPS-MEE plate is assumed to vary along $x$- and $y$-, respectively according to the relation as follows [77]:

$$\begin{aligned} u(x, y, z, t) &= u_0(x, y, t) + \left(z - \left\langle z - \frac{h}{2} \right\rangle\right)\theta_x(x, y, t) \\ &+ \left(\left\langle z - \frac{h}{2} \right\rangle - \langle z - h_{N+2} \rangle\right)\kappa_x(x, y, t) + \langle z - h_{N+2} \rangle \gamma_x(x, y, t) \\ v(x, y, z, t) &= v_0(x, y, t) + \left(z - \left\langle z - \frac{h}{2} \right\rangle\right)\theta_y(x, y, t) \\ &+ \left(\left\langle z - \frac{h}{2} \right\rangle - \langle z - h_{N+2} \rangle\right)\kappa_y(x, y, t) + \langle z - h_{N+2} \rangle \gamma_y(x, y, t) \end{aligned} \tag{7}$$

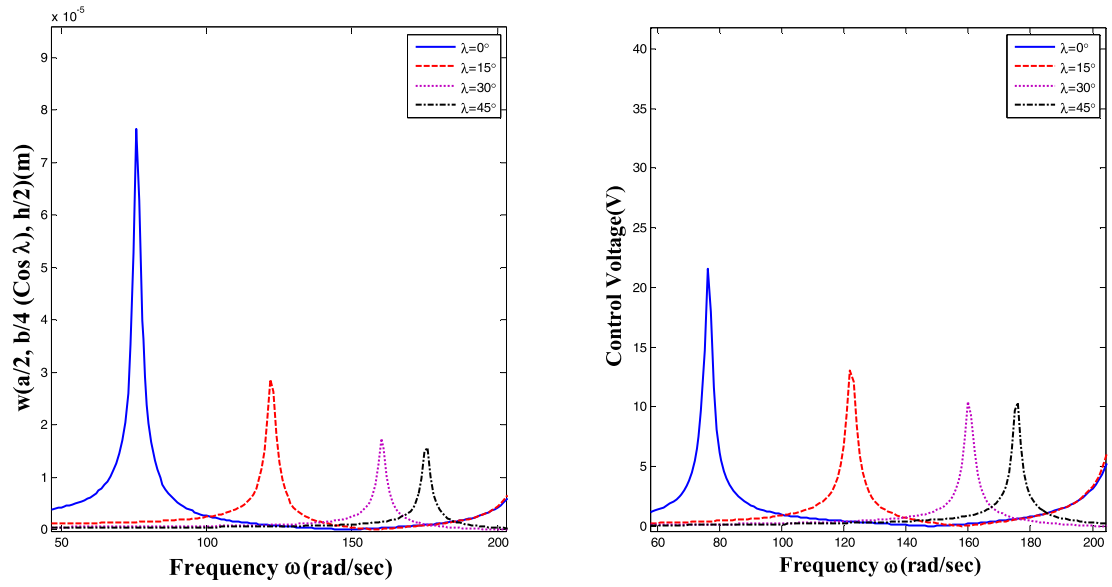


(c) $V_f = 0.3$

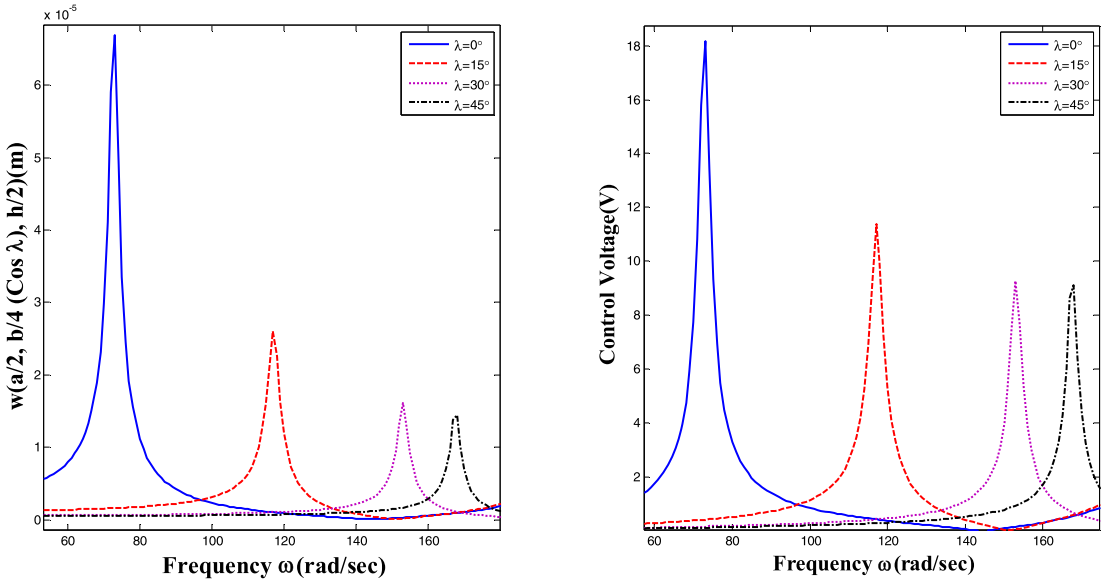


(d) $V_f = 0.2$

**Figure 4.** (Continued.)

Meanwhile, a higher order transverse displacement component $w$ is adopted to enhance the vertical attenuation of ACLD patch and it can be shown as follows:

$$w(x, y, z, t) = w_0(x, y, t) + z\theta_z(x, y, t) + z^2\kappa_z(x, y, t) \tag{8}$$

The mid-surface displacement components along $x$-, $y$- and $z$-axes are denoted by $u_0$, $v_0$ and $w_0$ respectively. Also, $\theta_x(\theta_y)$, $\kappa_x(\kappa_y)$and $\gamma_x$, $(\gamma_y)$ represents generalised rotations of the normal to mid-plane of the substrate, viscoelastic layer and piezoelectric patch about the $y$-axis ($x$-axis), respectively. Further, the terms $\theta_z$and$\kappa_z$ are the gradients of transverse displacements with respect to $z$-axis associated with the TPS-MEE plate and viscoelastic layer, respectively.

The governing equations of motion are derived incorporating the FE methods. A FE mesh with size $10 \times 10$ and eight noded isoparametric quadrilateral element is employed in this study. Invoking the principle of virtual work and skew transformations, the equations of motion of TPS-MEE plate embedded with ACLD treatment can be represented as [77]:

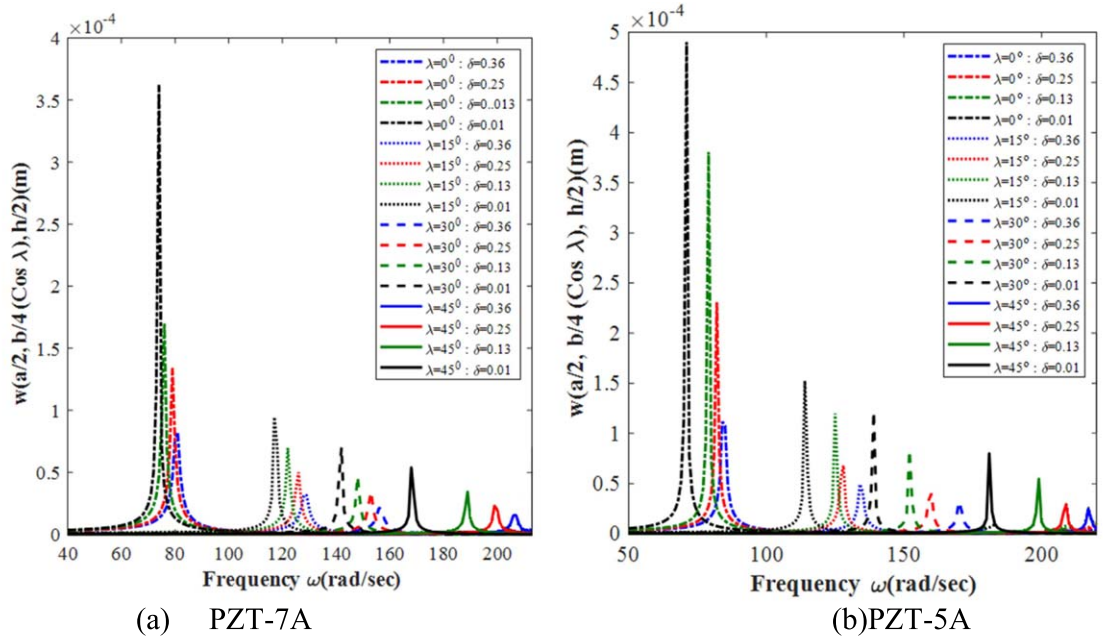


**Figure 5.** Effect of skew angle on the controlled linear frequency response function of deflection of TPS-MEE plate with different values of $\delta$.

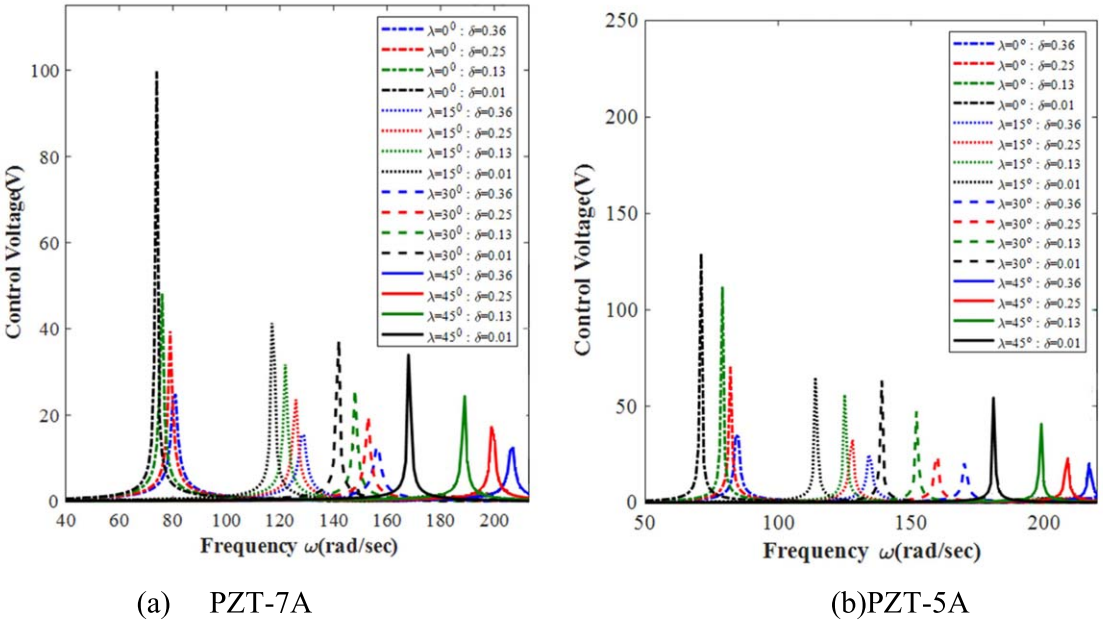


**Figure 6.** Effect of skew angle on the controlled linear frequency response function of control voltage of TPS-MEE plate with different values of $\delta$.

$$
\begin{aligned}
&[M]\{\ddot{X}\} + [K_{tt}]\{X\} + [K_{tr}]\{X_r\} + [K_{t\phi}]\{\phi\} + [K_{t\psi}]\{\psi\} \\
&\quad + \sum_{l=1}^{m}(\{F_{tp}^{l}\})K_d^l[U_t^l]\{\dot{X}\} = \{F\} \\
&[K_{tr}]^T\{X\} + [K_{rr}]\{X_r\} + [K_{r\phi}]\{\phi\} + [K_{r\psi}]\{\psi\} + \sum_{l=1}^{m}(\{F_{tp}^{l}\})K_d^l[U_t^l]\{\dot{X}\} = 0 \\
&[K_{t\phi}]^T\{X\} + [K_{r\phi}]^T\{X_r\} - [K_{\phi\phi}]\{\phi\} = 0 \\
&[K_{t\psi}]^T\{X\} + [K_{r\psi}]^T\{X_r\} - [K_{\psi\psi}]\{\psi\} = 0
\end{aligned} \tag{9}
$$

where, $[M]$ is the global mass matrix; $[K_{tt}]$, $[K_{tr}]$ and $[K_{rr}]$ the global elastic stiffness matrices; $[K_{t\phi}]$ and $[K_{r\phi}]$ the global coupled electro-elastic stiffness matrices; $[K_{t\psi}]$ and $[K_{r\psi}]$ the coupled magneto-elastic stiffness matrices;

**Table 4.** Effect of skew angle on the controlled linear frequency response function of maximum deflection ($\times 10^{-4}$ m) (PZT-7A).

| | $\delta = 0.36$ | | | | $\delta = 0.25$ | | | | $\delta = 0.13$ | | | | $\delta = 0.01$ | | | |
|---|---|---|---|---|---|---|---|---|---|---|---|---|---|---|---|---|
| | $\lambda = 0°$ | $\lambda = 15°$ | $\lambda = 30°$ | $\lambda = 45°$ | $\lambda = 0°$ | $\lambda = 15°$ | $\lambda = 30°$ | $\lambda = 45°$ | $\lambda = 0°$ | $\lambda = 15°$ | $\lambda = 30°$ | $\lambda = 45°$ | $\lambda = 0°$ | $\lambda = 15°$ | $\lambda = 30°$ | $\lambda = 45°$ |
| $V_f = 0.5$ | 9.741 | 4.558 | 2.979 | 2.485 | 17.98 | 6.722 | 3.983 | 2.727 | 18.63 | 7.711 | 5.441 | 4.488 | 4.487 | 1.11 | 0.8696 | 0.6553 |
| $V_f = 0.4$ | 8.25 | 3.168 | 2.155 | 1.592 | 11.58 | 5.007 | 3.44 | 2.709 | 17.05 | 6.964 | 4.674 | 4.175 | 3.665 | 0.9459 | 0.7016 | 0.5389 |
| $V_f = 0.3$ | 7.642 | 2.857 | 1.886 | 1.568 | 11.01 | 4.466 | 2.704 | 2.275 | 12.52 | 5.984 | 4.262 | 3.293 | 3.235 | 0.9137 | 0.6744 | 0.5292 |
| $V_f = 0.2$ | 6.696 | 2.6 | 1.617 | 1.448 | 10.38 | 3.92 | 2.687 | 2.269 | 12.08 | 5.447 | 3.818 | 2.464 | 2.477 | 0.9121 | 0.7364 | 0.5287 |

**Table 5.** Effect of skew angle on the controlled linear frequency response function of control voltage (PZT-7A).

| | $\delta = 0.36$ | | | | $\delta = 0.25$ | | | | $\delta = 0.13$ | | | | $\delta = 0.01$ | | | |
|---|---|---|---|---|---|---|---|---|---|---|---|---|---|---|---|---|
| | $\lambda = 0^\circ$ | $\lambda = 15^\circ$ | $\lambda = 30^\circ$ | $\lambda = 45^\circ$ | $\lambda = 0^\circ$ | $\lambda = 15^\circ$ | $\lambda = 30^\circ$ | $\lambda = 45^\circ$ | $\lambda = 0^\circ$ | $\lambda = 15^\circ$ | $\lambda = 30^\circ$ | $\lambda = 45^\circ$ | $\lambda = 0^\circ$ | $\lambda = 15^\circ$ | $\lambda = 30^\circ$ | $\lambda = 45^\circ$ |
| $V_f = 0.5$ | 31.22 | 23.03 | 18.42 | 18.19 | 56.25 | 33.45 | 24.18 | 20.05 | 56.66 | 37.5 | 28.51 | 26.73 | 130.3 | 52.73 | 50.16 | 49.16 |
| $V_f = 0.4$ | 24.88 | 15.17 | 12.59 | 12.37 | 32.37 | 23.59 | 19.7 | 18.38 | 48.21 | 31.77 | 25.9 | 25.03 | 102.00 | 41.36 | 37.29 | 33.93 |
| $V_f = 0.3$ | 21.61 | 13.03 | 10.41 | 10.34 | 31.86 | 19.87 | 15.8 | 14.58 | 33.04 | 25.49 | 22.03 | 18.38 | 78.05 | 36.86 | 33.05 | 29.73 |
| $V_f = 0.2$ | 18.17 | 11.37 | 9.265 | 9.118 | 26.99 | 16.55 | 13.98 | 13.69 | 30.05 | 21.97 | 18.57 | 15.7 | 130.3 | 59.77 | 34.73 | 32.48 |

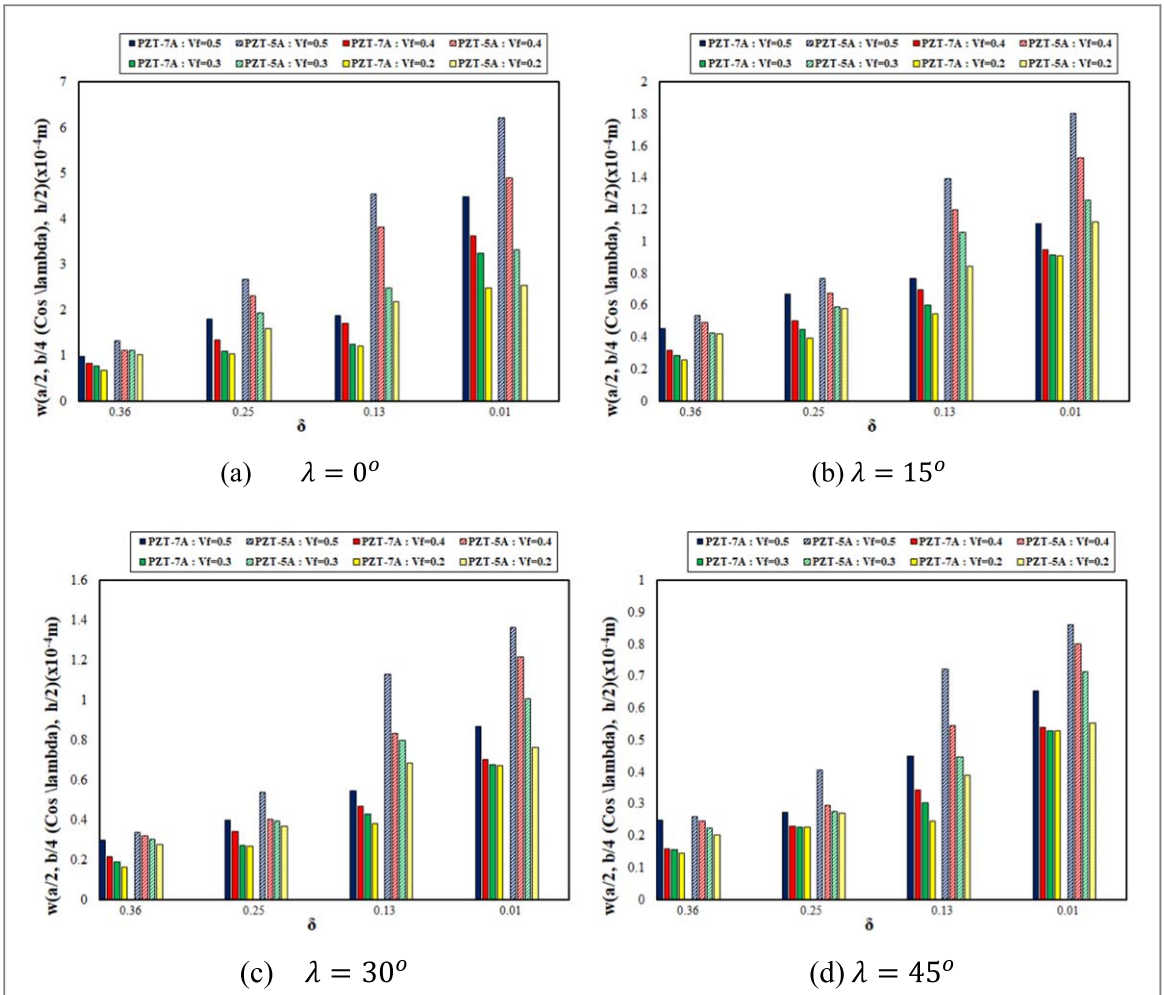


**Figure 7.** Effect of interphase material on the controlled linear frequency response function of deflection.

$[K_{\psi\psi}]$ and $[K_{\phi\phi}]$ the magnetic and electric stiffness matrices, and $\{F\}$ the mechanical force vector. The detailed derivation of FE formulation, explicit representation of the stiffness matrices and force vectors may refer to Ref. [77].

## 3. Problem description

The linear controlled frequency response of simply supported TPS-MEE plate with ACLD patch (figure 1(c)) is studied. To this end, the geometrical dimensions of TPS-MEE plate chosen for this study are: length $a = 0.5$ m, breadth $b = 0.5$ m, thickness $H = 3$ mm. The reference plane of the TPS-MEE plate is chosen at $z = 0$. The constraints employed in this study can be expressed as follows:

$$v_0^1 = w_0^1 = \theta_y^1 = \kappa_y^1 = \gamma_y^1 = \theta_z^1 = \kappa_z^1 = 0 \text{ at } x = y \tan\lambda \text{ and } x = a + y \tan\lambda$$
$$u_0 = w_0 = \theta_x = \kappa_x = \gamma_x = \theta_z = \kappa_z = 0 \text{ at } y = 0 \text{ and } y = b\cos\lambda \quad (10)$$

The ACLD patch is attached to the TPS-MEE substrate at its centre (figure 1(c)). Further, it is designed in such a manner that the constraining layer of 1–3 PZC patch is of thickness $h_p = 250$ $\mu$m and the constrained viscoelastic layer is of thickness $h_v = 50.8$ $\mu$m. The parameters $\lambda$ and $\alpha$ represents the skew angle of the TPS-MEE plate and piezoelectric fiber orientation angle of the 1–3 PZC patch. The TPS-MEE plate, is excited by force of 2 N at the position ($a/2$, $b/4\cos\lambda$, $H/2$).

## 4. Results and discussions

The influence of interphase on the damped frequency of ACLD treated TPS-MEE plate with various skew angles is demonstrated. The credibility of the FE formulation is justified in prior assuming the inactive state of ACLD. The results presented in tables 2 and 3 affirm that the proposed formulation properly accommodates the

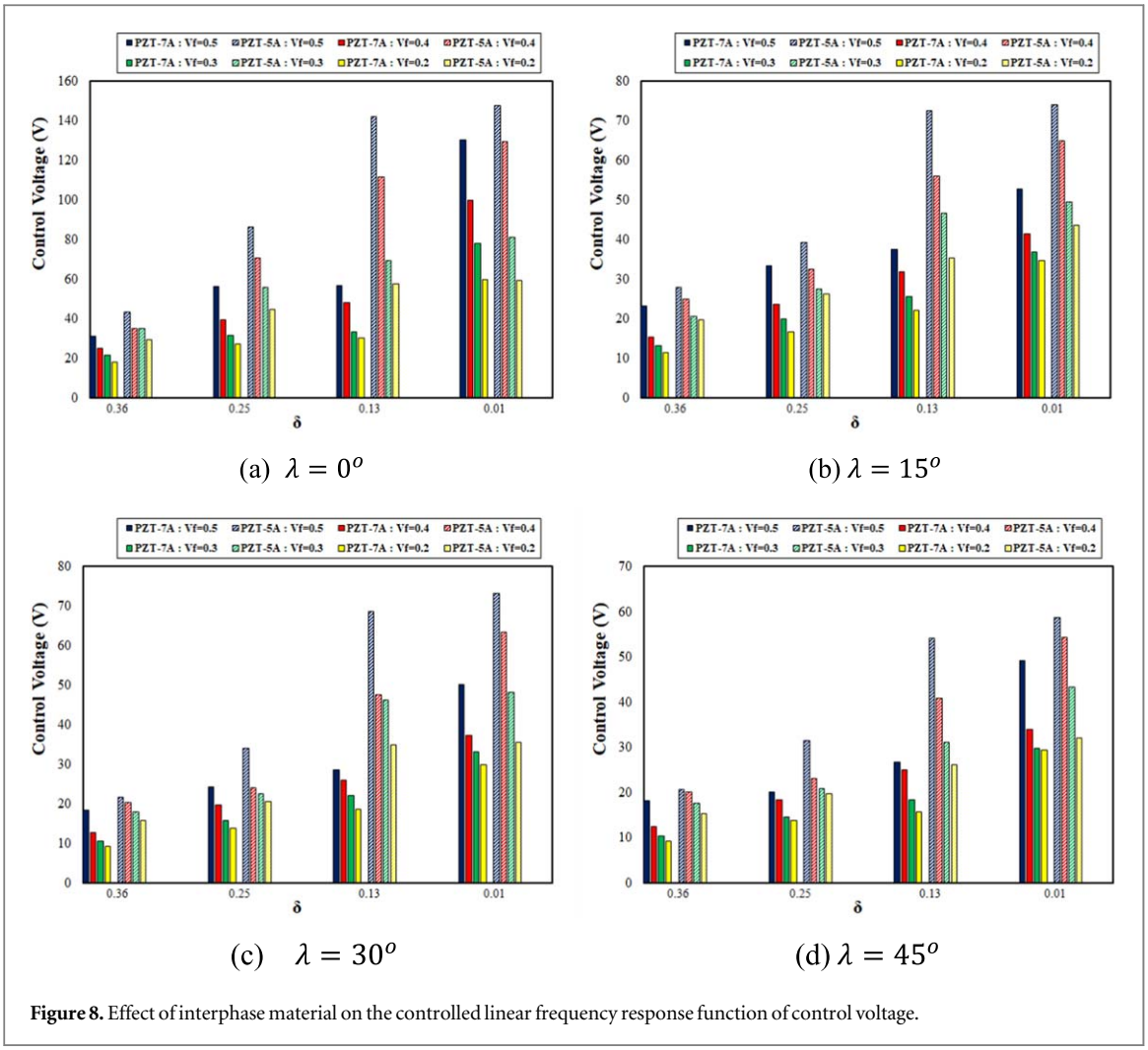


**Figure 8.** Effect of interphase material on the controlled linear frequency response function of control voltage.

coupling and geometrical skewness effects and yield reliable results. Therefore, it can be extended to evaluate the damped frequency response of TPS-MEE plate. In this analysis, unless mentioned otherwise, the interphase piezoelectric material PZT-7A, piezoelectric fiber orientation of 1–3 PZC patch $\alpha = 0$ °oriented in *yz*-plane, control gain $K_d = 600$ and a center ACLD patch is considered.

### 4.1. Effect of interphase thickness

The influence of interphase thickness ($\delta$) on the damped frequency of ACLD treated rectangular TPS-MEE plate ($\lambda = 0^{\circ}$) with a volume fraction $V_f =$ 0.2 to 0.5 is probed. Four different interphase thickness of PZT-7A viz, $\delta =$ 0.36, 0.25, 0.13 and 0.01 is considered for this study. From figures 2(a)–(d) it can be witnessed that the maximum linear frequency response functions for deflection is noticed for $\delta = 0.01$. The reason can be due to the minimum values of material constants, the TPS-MEE plate with $\delta = 0.01$ experiences minimal stiffness in contrast to the other interphase thickness. Therefore, the required control voltage to attenuate the vibrations are also higher for TPS-MEE plate with $\delta = 0.01$ as depicted in figure 3 for all the volume fractions.

### 4.2. Effect of skew angle

The degree of coupling associated with the TPS-MEE plate drastically changes with the geometrical skewness of the plate. Figures 4(a)–(d) encapsulate the influence of skew angle of TPS-MEE plate with $V_f =$ 0.2 to 0.5 and $\delta = 0.36$. It can be inferred from these plots that as the skew angle improve the linear frequency response functions for deflection and control voltage reduces. This can be attributed to the fact that the degree of coupling and hence the stiffness of the TPS-MEE plate improveswith the higher skew angle. The study is extended to evaluate the influence of interphase thickness associated with skew angle. From figures 5 and 6, it can be witnessed that with the improvement in the value of $\delta$ and skew angle $\lambda$, the attenuation capabilities of the plate significantly improves. Therefore it can be justified that both $\delta$ and skew angle $\lambda$ are the prominent parameters contributing to the damping characteristics of TPS-MEE plate.

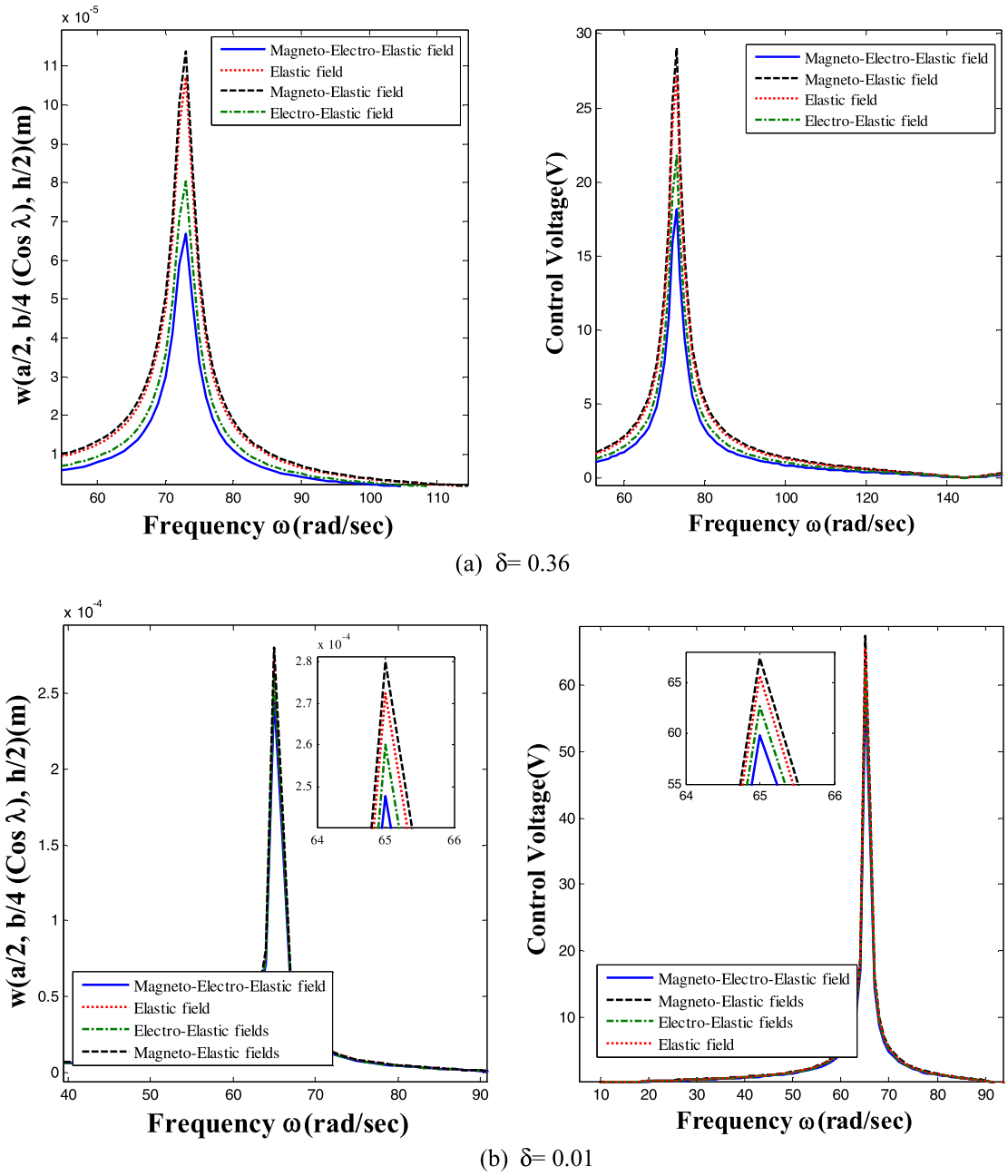


**Figure 9.** Effect of coupling associated with interphase thickness on the controlled linear frequency response function of deflection and control voltage ($V_f = 0.2$; PZT-7A; $\lambda = 45°$).

### 4.3. Effect of volume fraction

The effect of volume fraction of TPS-MEE material associated with different skew angle and interphase thickness on the linear frequency response functions of ACLD treated TPS-MEE plate is shown in tables 4 and 5 in terms of the maximum deflection and control voltage, respectively. It can be assessed from these results that as the volume fraction of TPS-MEE material increases from 0.2 to 0.5, the deflection and control voltage increases. This can be attributed to the fact that higher volume fraction of TPS-MEE material possess decreased percentage of $CoFe_2O_4$ phase which has superior elastic stiffness coefficient than the other phases of TPS-MEE material. In addition, the conclusions drawn in the previous section with respect to interphase thickness and skew angles can be observed here also.

### 4.4. Effect of interphase material

The piezoelectric material has a significant influence on the overall coupled characteristics of TPS-MEE material. An attempt has been made to assess the influence of prominent piezoelectric interphase material such as PZT-5A and PZT-7A on the linear frequency response functions of deflections and control voltage. From

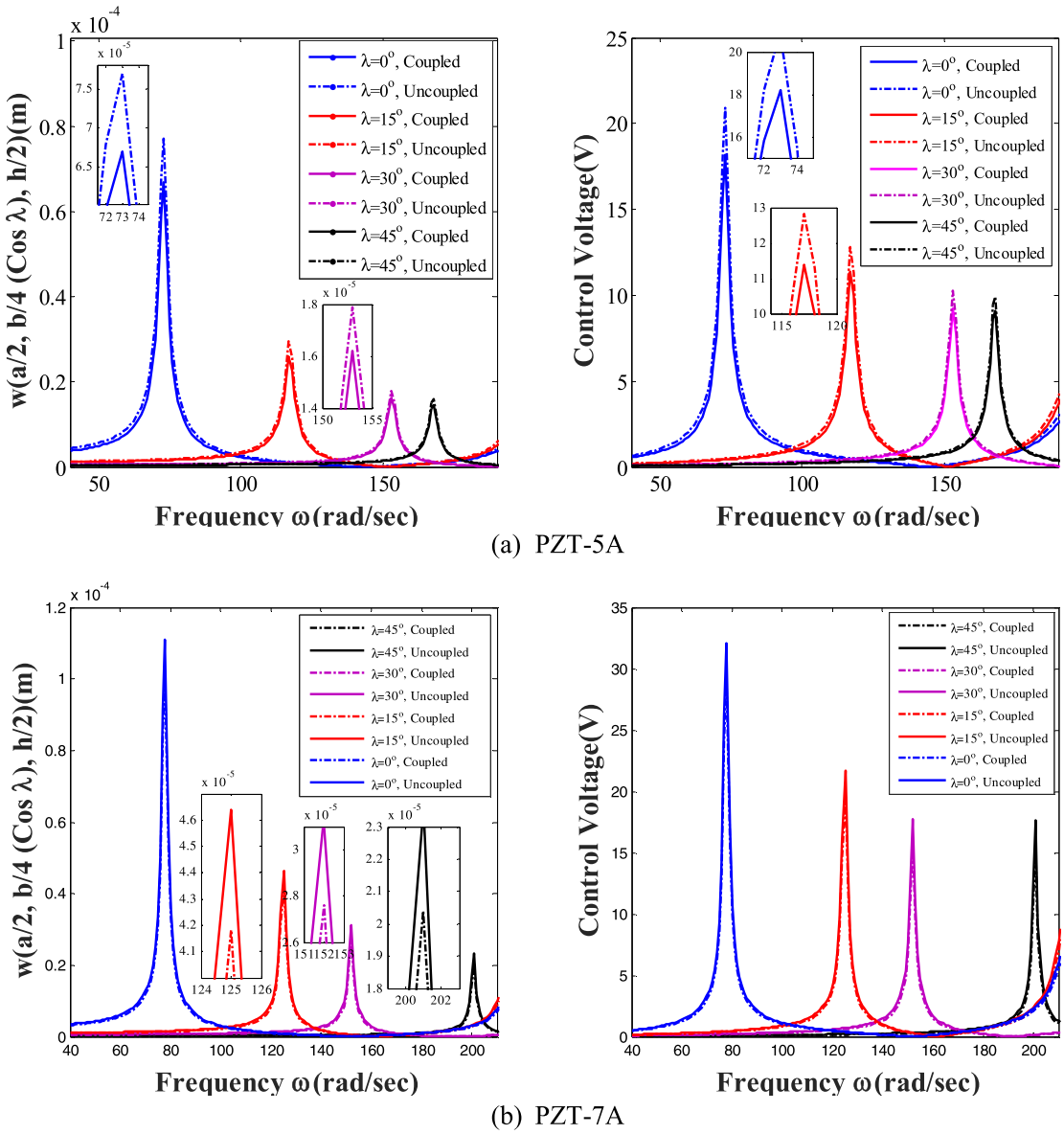


**Figure 10.** Effect of couplingassociated with the skew angle on the controlled linear frequency response function of deflection and control voltage.

figure 7, it is evident that in contrast to PZT-5A a predominant effect of PZT-7A is witnessed on the enhanced coupled frequency of the TPS-MEE plate. In other words, due to minimal stiffness, a higher deflection of the TPS-MEE plate with PZT-5A as the interphase material is noticed. The same trend is observed for the control voltage as well as shown in figure 8.

### 4.5. Effect of coupling

The coupling between magnetic, electric and elastic fields results in an effective vibration control of the TPS-MEE plate. However, when coupling between these fields are neglected, the structural behaviour of TPS-MEE plate marginally varies. Therefore, it is necessary to compare the linear frequency response of TPS-MEE plate with and without coupling effects. In addition, the contribution of interphase thickness and skew angles on the coupling effect needs to be determined. From figures 9 and 10, it can be seen that in contrast to lesser value of interphase thickness ($\delta = 0.01$), a higher value of interphase thickness ($\delta = 0.36$) results in a higher discrepancy of deflection and control voltage. In other words, the influence of coupling fields increases as the interphase thickness improves. In addition, magneto-elastic field tends to increase the deflection marginally more than the elastic fields. However, it is witnessed that when complete coupling is established between magnetic, electric and elastic fields, the maximum damping can be achieved. In addition, from tables 6–9 it can be seen that a higher percentage of contribution on the coupled behaviour of TPS-MEE plate is noticed for $\delta = 0.36$ which improves

**Table 6.** Effect of coupling on the controlled linear frequency response function of maximum deflection ($\times 10^{-4}$ m) (PZT-5A).

| Volume Fraction | $\lambda = 0^\circ$ | | | $\lambda = 15^\circ$ | | | $\lambda = 30^\circ$ | | | $\lambda = 45^\circ$ | | |
|---|---|---|---|---|---|---|---|---|---|---|---|---|
| | Coupled | Uncoupled | Error % | Coupled | Uncoupled | Error % | Coupled | Uncoupled | Error % | Coupled | Uncoupled | Error % |
| | | | | | | $\delta = 0.36$ | | | | | | |
| $V_f = 0.5$ | 1.323 | 1.424 | 7.651 | 0.535 | 0.588 | 9.835 | 0.338 | 0.378 | 11.851 | 0.259 | 0.289 | 11.965 |
| $V_f = 0.4$ | 1.116 | 1.208 | 8.254 | 0.494 | 0.545 | 10.322 | 0.319 | 0.358 | 12.354 | 0.247 | 0.278 | 12.456 |
| $V_f = 0.3$ | 1.112 | 1.205 | 8.348 | 0.425 | 0.470 | 10.614 | 0.303 | 0.341 | 12.501 | 0.223 | 0.252 | 12.781 |
| $V_f = 0.2$ | 1.014 | 1.107 | 9.125 | 0.418 | 0.464 | 11.122 | 0.276 | 0.314 | 13.689 | 0.203 | 0.233 | 14.836 |
| | | | | | | $\delta = 0.25$ | | | | | | |
| $V_f = 0.5$ | 2.665 | 2.858 | 7.256 | 0.767 | 0.838 | 9.236 | 0.535 | 0.594 | 11.156 | 0.406 | 0.454 | 11.810 |
| $V_f = 0.4$ | 2.310 | 2.487 | 7.648 | 0.679 | 0.745 | 9.682 | 0.400 | 0.446 | 11.576 | 0.294 | 0.330 | 12.365 |
| $V_f = 0.3$ | 1.925 | 2.084 | 8.239 | 0.589 | 0.648 | 10.125 | 0.391 | 0.439 | 12.251 | 0.276 | 0.311 | 12.698 |
| $V_f = 0.2$ | 1.595 | 1.733 | 8.651 | 0.578 | 0.639 | 10.633 | 0.367 | 0.414 | 12.923 | 0.269 | 0.304 | 13.157 |
| | | | | | | $\delta = 0.13$ | | | | | | |
| $V_f = 0.5$ | 4.541 | 4.842 | 6.633 | 1.393 | 1.514 | 8.688 | 1.129 | 1.249 | 10.620 | 0.721 | 0.805 | 11.667 |
| $V_f = 0.4$ | 3.807 | 4.086 | 7.344 | 1.199 | 1.307 | 9.002 | 0.833 | 0.926 | 11.203 | 0.546 | 0.613 | 12.326 |
| $V_f = 0.3$ | 2.478 | 2.665 | 7.559 | 1.059 | 1.159 | 9.454 | 0.799 | 0.892 | 11.632 | 0.448 | 0.504 | 12.644 |
| $V_f = 0.2$ | 2.184 | 2.359 | 8.012 | 0.843 | 0.932 | 10.555 | 0.684 | 0.768 | 12.318 | 0.390 | 0.441 | 13.115 |
| | | | | | | $\delta = 0.01$ | | | | | | |
| $V_f = 0.5$ | 6.211 | 6.597 | 6.213 | 1.803 | 1.949 | 8.109 | 1.366 | 1.469 | 9.996 | 0.860 | 0.959 | 11.588 |
| $V_f = 0.4$ | 4.903 | 5.229 | 6.669 | 1.525 | 1.656 | 8.628 | 1.217 | 1.345 | 10.568 | 0.801 | 0.899 | 12.265 |
| $V_f = 0.3$ | 3.311 | 3.553 | 7.326 | 1.261 | 1.380 | 9.453 | 1.008 | 1.121 | 11.189 | 0.714 | 0.804 | 12.598 |
| $V_f = 0.2$ | 2.544 | 2.744 | 7.856 | 1.121 | 1.228 | 9.588 | 0.762 | 0.849 | 11.366 | 0.554 | 0.626 | 13.085 |

**Table 7.** Effect of coupling on the controlled linear frequency response function of maximum control voltage (PZT-5A).

| Volume Fraction | $\lambda = 0^\circ$ | | | $\lambda = 15^\circ$ | | | $\lambda = 30^\circ$ | | | $\lambda = 45^\circ$ | | |
|---|---|---|---|---|---|---|---|---|---|---|---|---|
| | Coupled | Uncoupled | Error % | Coupled | Uncoupled | Error % | Coupled | Uncoupled | Error % | Coupled | Uncoupled | Error % |
| | | | | | | $\delta = 0.36$ | | | | | | |
| $V_f = 0.5$ | 43.405 | 46.759 | 7.727 | 27.858 | 30.625 | 9.933 | 21.681 | 24.276 | 11.969 | 20.544 | 23.026 | 12.084 |
| $V_f = 0.4$ | 34.931 | 37.843 | 8.336 | 24.794 | 27.378 | 10.425 | 20.356 | 22.895 | 12.477 | 20.156 | 22.691 | 12.580 |
| $V_f = 0.3$ | 34.816 | 37.751 | 8.431 | 20.512 | 22.710 | 10.720 | 17.912 | 20.173 | 12.626 | 17.518 | 19.779 | 12.908 |
| $V_f = 0.2$ | 29.447 | 32.161 | 9.216 | 19.553 | 21.749 | 11.233 | 15.710 | 17.882 | 13.825 | 15.352 | 17.654 | 14.984 |
| | | | | | | $\delta = 0.25$ | | | | | | |
| $V_f = 0.5$ | 86.405 | 92.737 | 7.328 | 39.331 | 42.999 | 9.328 | 34.080 | 37.919 | 11.267 | 31.551 | 35.314 | 11.928 |
| $V_f = 0.4$ | 70.521 | 75.968 | 7.724 | 32.544 | 35.726 | 9.778 | 24.009 | 26.816 | 11.691 | 23.064 | 25.944 | 12.488 |
| $V_f = 0.3$ | 55.890 | 60.540 | 8.321 | 27.558 | 30.376 | 10.226 | 22.405 | 25.177 | 12.373 | 20.749 | 23.410 | 12.824 |
| $V_f = 0.2$ | 44.564 | 48.457 | 8.737 | 26.169 | 28.979 | 10.739 | 20.482 | 23.155 | 13.052 | 19.592 | 22.195 | 13.288 |
| | | | | | | $\delta = 0.13$ | | | | | | |
| $V_f = 0.5$ | 142.121 | 151.642 | 6.699 | 72.468 | 78.826 | 8.774 | 68.556 | 75.909 | 10.726 | 54.110 | 60.486 | 11.783 |
| $V_f = 0.4$ | 111.546 | 119.819 | 7.417 | 56.052 | 61.148 | 9.092 | 47.414 | 52.778 | 11.315 | 40.765 | 45.839 | 12.449 |
| $V_f = 0.3$ | 69.144 | 74.422 | 7.634 | 46.730 | 51.192 | 9.548 | 46.148 | 51.569 | 11.748 | 31.062 | 35.028 | 12.770 |
| $V_f = 0.2$ | 57.652 | 62.317 | 8.092 | 35.285 | 39.046 | 10.660 | 34.849 | 39.184 | 12.441 | 26.158 | 29.622 | 13.246 |
| | | | | | | $\delta = 0.01$ | | | | | | |
| $V_f = 0.5$ | 147.502 | 156.757 | 6.275 | 74.112 | 80.181 | 8.190 | 73.136 | 80.519 | 10.095 | 58.710 | 65.581 | 11.703 |
| $V_f = 0.4$ | 129.445 | 138.164 | 6.735 | 64.951 | 70.611 | 8.714 | 63.344 | 70.105 | 10.673 | 54.335 | 61.065 | 12.387 |
| $V_f = 0.3$ | 81.125 | 87.127 | 7.399 | 49.452 | 54.173 | 9.547 | 48.269 | 53.723 | 11.300 | 43.313 | 48.824 | 12.723 |
| $V_f = 0.2$ | 59.468 | 64.186 | 7.934 | 43.526 | 47.741 | 9.683 | 35.638 | 39.729 | 11.479 | 31.970 | 36.195 | 13.215 |

**Table 8.** Effect of coupling on the controlled linear frequency response function of maximum deflection ($\times 10^{-4}$ m) (PZT-7A).

| | $w(\times 10^{-4}$ m) | | | | | | | | | | | |
|---|---|---|---|---|---|---|---|---|---|---|---|---|
| | $\lambda = 0°$ | | | $\lambda = 15°$ | | | $\lambda = 30°$ | | | $\lambda = 45°$ | | |
| Volume Fraction | Coupled | Uncoupled | Error% | Coupled | Uncoupled | Error% | Coupled | Uncoupled | Error% | Coupled | Uncoupled | Error % |
| | | | | | | $\delta = 0.36$ | | | | | | |
| $V_f = 0.5$ | 0.974 | 1.0476 | 7.552 | 0.456 | 0.501 | 9.796 | 0.298 | 0.333 | 11.704 | 0.249 | 0.279 | 11.871 |
| $V_f = 0.4$ | 0.825 | 0.893 | 8.193 | 0.317 | 0.349 | 10.267 | 0.216 | 0.242 | 12.265 | 0.159 | 0.179 | 12.352 |
| $V_f = 0.3$ | 0.764 | 0.827 | 8.266 | 0.286 | 0.316 | 10.554 | 0.187 | 0.211 | 12.452 | 0.157 | 0.177 | 12.698 |
| $V_f = 0.2$ | 0.670 | 0.731 | 9.065 | 0.260 | 0.287 | 11.050 | 0.162 | 0.184 | 13.591 | 0.145 | 0.166 | 14.763 |
| | | | | | | $\delta = 0.25$ | | | | | | |
| $V_f = 0.5$ | 1.798 | 1.926 | 7.124 | 0.672 | 0.733 | 9.124 | 0.398 | 0.442 | 11.058 | 0.272 | 0.304 | 11.785 |
| $V_f = 0.4$ | 1.342 | 1.443 | 7.548 | 0.501 | 0.549 | 9.568 | 0.343 | 0.383 | 11.569 | 0.230 | 0.258 | 12.254 |
| $V_f = 0.3$ | 1.095 | 1.184 | 8.158 | 0.447 | 0.492 | 10.015 | 0.270 | 0.303 | 12.125 | 0.227 | 0.256 | 12.620 |
| $V_f = 0.2$ | 1.038 | 1.126 | 8.511 | 0.392 | 0.4333 | 10.542 | 0.267 | 0.301 | 12.851 | 0.226 | 0.255 | 13.016 |
| | | | | | | $\delta = 0.13$ | | | | | | |
| $V_f = 0.5$ | 1.863 | 1.985 | 6.549 | 0.771 | 0.837 | 8.547 | 0.544 | 0.601 | 10.513 | 0.449 | 0.501 | 11.564 |
| $V_f = 0.4$ | 1.705 | 1.829 | 7.265 | 0.696 | 0.758 | 8.896 | 0.467 | 0.519 | 11.125 | 0.343 | 0.385 | 12.205 |
| $V_f = 0.3$ | 1.252 | 1.346 | 7.503 | 0.598 | 0.654 | 9.365 | 0.426 | 0.475 | 11.541 | 0.302 | 0.340 | 12.584 |
| $V_f = 0.2$ | 1.208 | 1.303 | 7.857 | 0.545 | 0.599 | 9.963 | 0.381 | 0.428 | 12.265 | 0.246 | 0.278 | 13.000 |
| | | | | | | $\delta = 0.01$ | | | | | | |
| $V_f = 0.5$ | 4.487 | 4.763 | 6.149 | 1.11 | 1.199 | 8.036 | 0.869 | 0.956 | 9.985 | 0.655 | 0.734 | 12.102 |
| $V_f = 0.4$ | 3.624 | 3.863 | 6.603 | 0.946 | 1.027 | 8.541 | 0.701 | 0.774 | 10.455 | 0.539 | 0.606 | 12.488 |
| $V_f = 0.3$ | 3.235 | 3.469 | 7.257 | 0.914 | 0.995 | 8.942 | 0.674 | 0.748 | 11.050 | 0.529 | 0.598 | 12.950 |
| $V_f = 0.2$ | 2.477 | 2.669 | 7.789 | 0.912 | 0.994 | 9.026 | 0.672 | 0.747 | 11.200 | 0.528 | 0.597 | 12.963 |

**Table 9.** Effect of coupling on the controlled linear frequency response function of maximum control voltage (PZT-5A).

| Volume Fraction | $\lambda = 0^\circ$ | | | $\lambda = 15^\circ$ | | | $\lambda = 30^\circ$ | | | $\lambda = 45^\circ$ | | |
|---|---|---|---|---|---|---|---|---|---|---|---|---|
| | Coupled | Uncoupled | Error % | Coupled | Uncoupled | Error % | Coupled | Uncoupled | Error% | Coupled | Uncoupled | Error % |
| | | | | | | $\delta = 0.36$ | | | | | | |
| $V_f = 0.5$ | 31.221 | 33.613 | 7.660 | 23.036 | 25.315 | 9.896 | 18.424 | 20.602 | 11.821 | 18.196 | 20.377 | 11.989 |
| $V_f = 0.4$ | 24.885 | 26.931 | 8.225 | 15.214 | 16.777 | 10.278 | 12.595 | 14.155 | 12.387 | 12.372 | 13.915 | 12.475 |
| $V_f = 0.3$ | 21.614 | 23.401 | 8.266 | 13.039 | 14.430 | 10.668 | 10.418 | 11.728 | 12.576 | 10.346 | 11.673 | 12.825 |
| $V_f = 0.2$ | 18.173 | 19.831 | 9.122 | 11.372 | 12.648 | 11.223 | 9.265 | 10.536 | 13.727 | 9.118 | 10.477 | 14.910 |
| | | | | | | $\delta = 0.25$ | | | | | | |
| $V_f = 0.5$ | 56.250 | 60.282 | 7.168 | 33.457 | 36.524 | 9.168 | 24.184 | 26.885 | 11.168 | 20.052 | 22.438 | 11.903 |
| $V_f = 0.4$ | 39.452 | 42.567 | 7.896 | 23.594 | 25.856 | 9.588 | 19.706 | 22.008 | 11.685 | 17.174 | 19.299 | 12.376 |
| $V_f = 0.3$ | 31.373 | 33.951 | 8.220 | 19.878 | 21.898 | 10.165 | 15.836 | 17.775 | 12.463 | 14.583 | 16.442 | 12.746 |
| $V_f = 0.2$ | 26.996 | 29.316 | 8.596 | 16.55 | 18.299 | 10.569 | 13.811 | 15.604 | 12.979 | 13.67 | 15.467 | 13.146 |
| | | | | | | $\delta = 0.13$ | | | | | | |
| $V_f = 0.5$ | 56.881 | 60.642 | 6.612 | 37.502 | 40.735 | 8.621 | 28.513 | 31.540 | 10.618 | 26.737 | 29.859 | 11.679 |
| $V_f = 0.4$ | 48.218 | 48.839 | 7.288 | 31.775 | 34.606 | 8.910 | 25.907 | 28.818 | 11.236 | 24.335 | 27.335 | 12.327 |
| $V_f = 0.3$ | 33.049 | 35.561 | 7.602 | 25.493 | 27.903 | 9.452 | 22.038 | 24.607 | 11.656 | 18.376 | 20.712 | 12.709 |
| $V_f = 0.2$ | 30.053 | 32.430 | 7.910 | 21.976 | 24.179 | 10.025 | 18.573 | 20.873 | 12.387 | 15.709 | 17.772 | 13.130 |
| | | | | | | $\delta = 0.01$ | | | | | | |
| $V_f = 0.5$ | 130.319 | 138.393 | 6.196 | 52.733 | 57.003 | 8.096 | 50.165 | 55.224 | 10.085 | 49.165 | 55.174 | 12.223 |
| $V_f = 0.4$ | 99.742 | 106.717 | 6.993 | 41.365 | 44.940 | 8.644 | 37.294 | 41.232 | 10.559 | 33.932 | 38.211 | 12.612 |
| $V_f = 0.3$ | 78.056 | 83.774 | 7.326 | 36.868 | 40.194 | 9.023 | 33.058 | 36.747 | 11.161 | 29.734 | 33.623 | 13.0795 |
| $V_f = 0.2$ | 59.770 | 64.465 | 7.856 | 34.732 | 37.901 | 9.123 | 29.887 | 33.268 | 11.312 | 29.301 | 33.137 | 13.0926 |

with higher skew angle and volume fraction. The schematic representation of discrepancies existing between coupled and uncoupled values of deflection and control voltage corresponding to skewed TPS-MEE plate with $V_f = 0.2$ and $\delta = 0.36$ for both PZT-5A and PZT-7A is shown in figures 10(a) and (b), respectively.

## 5. Conclusions

In this article the damped linear frequency response of active constrained layer damping (ACLD) treated three phase smart magneto electro elastic (TPS-MEE) plate with skewed edges is investigated through finite element methods. The TPS-MEE plate is composed of carbon fiber/piezoelectric interphase/piezomagnetic material. The equations of motion are derived using the principle of virtual work. The numerical results suggest that the attenuation capability of TPS-MEE plate improves with the increase in the interphase thickness. An improvement in the volume fraction results in increased damping phenomenon. In addition, PZT-7A is found to be a better interphase material when compared to PZT-5A. The linear frequency response functions for deflection and control voltage increases with the reduction in the skew angle of the plate. Finally, the results reveal that higher couplings between magnetic, electric and elastic fields are noticed for TPS-MEE plate with higher interphase thickness$\delta = 0.36$, skew angle $\lambda = 45^\circ$ and $V_f = 0.2$. It is firmly believed that the results of this article will serve as benchmark for upcoming researches on TPS-MEE structural analysis.

## ORCID iDs

M Vinyas https://orcid.org/0000-0001-8394-1321

## References

[1] Van Run A M J G, Terrell D R and Scholing J H 1974 An *in situ* grown eutectic magnetoelectric composite material *J. Mater. Sci.* **9** 1710–4
[2] Boomgaard J V D, Van Run A M J G and Van Suchtelen J 1976 Piezoelectric-piezomagnetic composites with magnetoelectric effect *Ferroelectrics* **14** 727–8
[3] Boomgaard J V D and Born R A J 1978 A sintered magnetoelectric composite material $BaTiO_3$-Ni (Co, Mn) $Fe_2O_4$ *J. Mater. Sci.* **13** 1538–48
[4] Dai Q and Ng K 2012 Investigation of electromechanical properties of piezoelectric structural fiber composites with micromechanics analysis and finite element modeling *Mech. Mater.* **53** 29–46
[5] Bakkali A, Azrar L and Alghamdi A A A 2013 Micromechanical modeling of magnetoelectroelastic composite materials with multicoated inclusions and functionally graded interphases *J. Intell. Mater. Syst. Struct.* **24** 1754–69
[6] Bakkali A, Azrar L and Alghamdi A A A 2012 Multi-coated magneto electro elastic composites with functionally graded interphases *MATEC Web of Conferences, EDPSciences* 09001-1–09001-4 pp (https://doi.org/10.1051/matecconf/20120109001)
[7] Espinosa-Almeyda Y *et al* 2017 Influence of imperfect interface and fiber distribution on the antiplane effective magneto-electro-elastic properties for fiber reinforced composites *Int. J. Solids Struct.* **112** 155–68
[8] Guinovart-Díaz R, Rodríguez-Ramos R, Bravo-Castillero J, Sabina F J, Galindo G M and Wang Y-S 2013 Plane magneto-electro-elastic moduli of fiber composites with interphase *Mech. Adv. Mater. Struct.* **20** 552–63
[9] Espinosa-Almeyda Y *et al* 2014 Antiplane magneto-electro-elastic effective properties of three-phase fiber composites *Int. J. Solids Struct.* **51** 3508–21
[10] Jiang C P and Cheung Y K 2001 An exact solution for the three-phase piezoelectric cylinder model under anti plane shear and its applications to piezoelectric composites *Int. J. Solids Struct.* **38** 4777–96
[11] Sladek J, Sladek V, Repka M, Kasala J and Bishay P 2017 Evaluation of effective material properties in magneto-electro-elastic composite materials *Compos. Struct.* **174** 176–86
[12] Huang J H 1998 Analytical predictions for the magnetoelectric coupling in piezomagnetic materials reinforced by piezoelectric ellipsoidal inclusions *Phys. Rev.* B **58** 12–5
[13] Huang J H and Kuo W-S 1997 The analysis of piezoelectric/piezomagnetic composite materials containing ellipsoidal inclusions *J. Appl. Phys.* **81** 1378–86
[14] Odegard G M 2004 Constitutive modeling of piezoelectric polymer composites *Acta. Materialia* **52** 5315–30
[15] Shen L and Li J 2005 Homogenization of a fibre/sphere with an in homogeneous interphase for the effective elastic moduli of composites *Proceedings of the Royal Society A: Mathematical, Physical and Engineering Sciences* **461** 1475–504
[16] Sevostianov I and Kachanov M 2006 Homogenization of a nanoparticle with graded interface *Int. J. Fract.* **139** 121–7
[17] Aboudi J 2001 Micromechanical analysis of fully coupled electro-magneto-thermo-elastic multiphase composites *Smart Mater. Struct.* **10** 867–77
[18] Koutsawa Y 2015 Overall thermo-magneto-electro-elastic properties of multiferroics composite materials with arbitrary heterogeneities spatial distributions *Compos. Struct.* **133** 764–73
[19] Koutsawa Y, Belouettar S, Makradi A and Tiem S 2011 Generalization of the micromechanicsmulti-coating approach to coupled fields composite materials with eigen fields: effective properties *Mech. Res. Commun.* **38** 45–51
[20] Koutsawa Y, Belouettar S, Makradi A and Tiem S 2012 X-FEM implementation of VAMUCH: application to active structural fiber multifunctional composite materials *Compos. Struct.* **94** 1297–304
[21] Li J Y 2000 Magneto electro elastic multi-inclusion and inhomogeneity problems and their applications in composite materials *Int. J. Eng. Sci.* **38** 1993–2011
[22] Giordano S, Goueygou M, Tiercelin N, Talbi A, Pernod P and Preobrazhensky V 2014 Magneto-electro-elastic effective properties of multilayered artificial multiferroics with arbitrary lamination direction *Int. J. Eng. Sci.* **78** 134–53

[23] Lee J, Boyd J G and Lagoudas D C 2005 Effective properties of three-phase electro-magneto-elastic composites *Int. J. Eng. Sci.* **43** 790–825
[24] Tang T and Yu W 2008 Variational asymptotic homogenization of heterogeneous electro magneto elastic materials *Int. J. Eng. Sci.* **46** 741–57
[25] Tang T and Yu W 2007 A variational asymptotic micromechanics model for predicting conductivities of composite materials *Journal of Mechanics of Materials and Structures* **2** 1813–30
[26] Tang T and Yu W 2008 Variational asymptotic micromechanics modeling of heterogeneous piezoelectric materials *Mech. Mater.* **40** 812–24
[27] Yu W and Tang T 2007 Variational asymptotic method for unit cell homogenization of periodically heterogeneous materials *Int. J. Solids Struct.* **44** 3738–55
[28] Yu W and Tang T 2007 A variational asymptotic micromechanics model for predicting thermo elastic properties of heterogeneous materials *Int. J. Solids Struct.* **44** 7510–25
[29] Challagulla K S and Georgiades A V 2011 Micromechanical analysis of magneto-electro-thermo-elastic composite materials with applications to multilayered structures *Int. J. Eng. Sci.* **49** 85–104
[30] Sixto-Camacho L M, Bravo-Castillero J, Brenner R, Guinovart-Díaz R, Mechkour H, Rodríguez-Ramos R and Sabina F J 2013 Asymptotic homogenization of periodic thermo-magneto-electro-elastic heterogeneous media *Computers and Mathematics with Applications* **66** 2056–74
[31] Hadjiloizi D A, Georgiades A V, Kalamkarov A L and Jothi S 2013 Micromechanical modeling of piezo-magneto-thermo-elastic composite structures: I. Theory *European Journal of Mechanics—A/Solids* **39** 298–312
[32] Hadjiloizi D A, Georgiades A V, Kalamkarov A L and Jothi S 2013 Micromechanical modeling of piezo-magneto-thermo-elastic composite structures: II. Applications *European Journal of Mechanics—A/Solids* **39** 313–27
[33] Pan E 2001 Exact solution for simply supported and multilayered magneto-electro-elastic plates *J. Appl. Mech.* **68** 608–18
[34] Pan E and Heyliger P R 2002 Free vibrations of simply supported and multilayered magneto-electro-elastic plates *J. Sound Vib.* **252** 429–42
[35] Lage R G, Soares C M, Soares C A and Reddy J N 2004 Layerwise partial mixed finite element analysis of magneto-electro-elastic plates *Comput. Struct.* **82** 1293–301
[36] Vinyas M 2019 A higher order free vibration analysis of carbon nanotube-reinforced magneto-electro-elastic plates using finite element methods *Composites Part* B **158** 286–301
[37] Wang J, Chen L and Fang S 2003 State vector approach to analysis of multilayered magneto-electro-elastic plates *Int. J. Solids Struct.* **40** 1669–80
[38] Chen W Q, Lee K Y and Ding H J 2005 On free vibration of non-homogeneous transversely isotropic magneto-electro-elastic plates *J. Sound Vib.* **279** 237–51
[39] Zhou Y Y, Lü C F and Chen W Q 2012 Bulk wave propagation in layered piezomagnetic/piezoelectric plateswith initial stresses or interface imperfections *Compos. Struct.* **94** 2736–45
[40] Chen J Y, Heyliger P R and Pan E 2014 Free vibration of three-dimensional multilayered magneto-electro-elastic plates under combined clamped/free boundary conditions *J. Sound Vib.* **333** 4017–29
[41] Xin L and Hu Z 2015 Free vibration of simply supported and multilayered magneto-electro-elastic plates *Compos. Struct.* **121** 344–50
[42] Ramirez F, Heyliger P R and Pan E 2006 Free vibration response of two-dimensional magneto-electro-elastic laminated plates *J. Sound Vib.* **292** 626–44
[43] Huang D J, Ding H J and Chen W Q 2007 Analytical solution for functionally graded magneto-electro-elastic plane beams *Int. J. Eng. Sci.* **45** 467–85
[44] Annigeri A R, Ganesan N and Swarnamani S 2007 Free vibration behavior of multiphase and layered magneto-electro-elastic beam *J. Sound Vib.* **299** 44–63
[45] Vinyas M and Kattimani S C 2018 Finite element evaluation of free vibration characteristics of magneto-electro-elastic rectangular plates in hygrothermal environment using higher-order shear deformation theory *Compos. Struct.* **202** 1339–52
[46] Vinyas M, Piyush J S and Kattimani S C 2018 Influence of coupled fields on free vibration and static behavior of functionally graded magneto-electro-thermo-elastic plate *J. Intell. Mater. Syst. Struct.* **29** 1430–55
[47] Vinyas M, Nischith G, Loja M A R, Ebrahimi F and Duc N D 2019 Numerical analysis of the vibration response of skew magneto-electro-elastic plates based on the higher-order shear deformation theory *Compos. Struct.* **214** 132–42
[48] Moita J M S, Soares C M M and Soares C A M 2009 Analyses of magneto-electro-elastic plates using a higher order finite element model *Compos. Struct.* **91** 421–6
[49] Bhangale R K and Ganesan N 2006 Free vibration of simply supported functionally graded and layered magneto-electro-elastic plates by finite element method *Journal of Sound and Vibrations* **294** 1016–38
[50] JSladek J, Sladek V, Krahulec S and Pan E 2013 The MLPG analyses of large deflections of magnetoelectroelastic plates *Eng. Anal. Boundary Elem.* **37** 673–82
[51] Vinyas M and Kattimani S C 2017 Static studies of stepped functionally graded magneto-electro-elastic beam subjected to different thermal loads *Compos. Struct.* **163** 216–37
[52] Chen W Q and Lee K Y 2003 Alternative state space formulations for magnetoelectric thermoelasticity with transverse isotropy and the application to bending analysis of nonhomogeneous plates *Int. J. Solids Struct.* **40** 5689–705
[53] Vinyas M and Kattimani S C 2017 A finite element based assessment of static behavior of multiphase magneto-electro-elastic beams under different thermal loading *Struct. Eng. Mech.* **62** 519–35
[54] Vinyas M and Kattimani S C 2017 Static behavior of thermally loaded multilayered magneto-electro-elastic beam *Struct. Eng. Mech.* **63** 481–95
[55] Vinyas M and Kattimani S C 2017 Multiphysics response of magneto-electro-elastic beams in thermo-mechanical environment *Coupled Systems Mechanics* **6** 351–68
[56] Vinyas M and Kattimani S C 2017 A 3D finite element static and free vibration analysis of magneto-electro-elastic beam *Coupled System Mechanics* **6** 465–85
[57] Vinyas M and Kattimani S C 2017 Static analysis of stepped functionally graded magneto-electro-elastic plates in thermal environment: a finite element study *Compos. Struct.* **178** 63–86
[58] Vinyas M and Kattimani S C 2017 Hygrothermal analysis of magneto-electro-elastic plate using 3D finite element analysis *Compos. Struct.* **180** 617–37
[59] Vinyas M and Kattimani S C 2018 Investigation of the effect of $BaTiO_3/CoFe_2O_4$ particle arrangement on the static response of magneto-electro-thermo-elastic plates *Compos. Struct.* **185** 51–64

[60] Vinyas M, Kattimani S C, Loja M A R and Vishwas M 2018 Effect of $BaTiO_3/CoFe_2O_4$ micro-topological textures on the coupled static behaviour of magneto-electro-thermo-elastic beams indifferent thermal environment *Material Research Express* **5** 125702
[61] Vinyas M, Kattimani S C and Joladarashi S 2018 Hygrothermal coupling analysis of magneto-electroelastic beams using finite element methods *J. Therm. Stresses* **41** 1063–79
[62] Newnham R E, Bowen L J, Klicker K A and Cross L E 1980 Composite piezoelectric transducers *Mater. Des.* **2** 93–106
[63] Ray M C and Pradhan A K 2007 On the use of vertically reinforced 1–3 piezoelectric composites for hybrid damping of laminated composite plates *Mech. Adv. Mater. Struct.* **14** 245–61
[64] Panda S and Ray M C 2009 Active control of geometrically nonlinear vibrations of functionally graded laminated composite plates using piezoelectric fiber reinforced composites *J. Sound Vib.* **325** 186–205
[65] Panda S and Ray M C 2006 Nonlinear analysis of smart functionally graded plates integrated with a layer of piezoelectric fiber reinforced composite *Smart Mater. Struct.* **15** 1595–604
[66] Kumar R S and Ray M C 2016 Smart damping of geometrically nonlinear vibrations of functionally graded sandwich plates using 1–3 piezoelectric composites *Mech. Adv. Mater. Struct.* **23** 652–69
[67] Ray M C and Mallik N 2005 Performance of smart damping treatment using piezoelectric fiber reinforced composites *American Institute of Aeronautics and Astronautics* **43** 184–93
[68] Ray M C and Pradhan A K 2006 Performance of vertically reinforced 1–3 piezoelectric composites for active damping of smart structures *Smart Mater. Struct.* **15** 631–41
[69] Shivakumar J and Ray M C 2008 Nonlinear analysis of smart cross-ply composite plates integrated with a distributed piezoelectric fiber reinforced composite actuator *Mech. Adv. Mater. Struct.* **15** 40–52
[70] Kumar R S and Ray M C 2012 Active constrained layer damping of smart laminated composite sandwich plates using 1–3 piezoelectric composites *Int. J. Mech. Mater. Des.* **8** 197–218
[71] Kumar R S and Ray M C 2012 Active constrained layer damping of geometrically nonlinear vibrations of smart laminated composite sandwich plates using 1–3 piezoelectric composites *Int. J. Mech. Mater. Des.* **8** 359–80
[72] Kanasogi R M and Ray M C 2013 Active constrained layer damping of smart skew laminated composite plates using 1–3 piezoelectric composites *Journal of Composites* **2013** 1–17
[73] Kattimani S C and Ray M C 2014a Smart damping of geometrically nonlinear vibrations of magneto-electro-elastic plates *Compos. Struct.* **114** 51–63
[74] Kattimani S C and Ray M C 2015 Control of geometrically nonlinear vibrations of functionally graded magneto-electro-elastic plates *Int. J. Mech. Sci.* **99** 154–67
[75] Kattimani S C and Ray M C 2018 Vibration control of multiferroic fibrous composite plates using active constrained layer damping *Mech. Syst. Sig. Process.* **106** 334–54
[76] Kattimani S C and Ray M C 2014 Active control of large amplitude vibrations of smart magneto–electro–elastic doubly curved shells *Int. J. Mech. Mater. Des.* **10** 351–78
[77] Vinyas M 2019 Vibration control of skew magneto-electro-elastic plates using active constrained layer damping *Compos. Struct.* **208** 600–17
[78] Vinyas M and Kattimani S C 2019 Finite element simulation of controlled frequency response of skew multiphase magneto-electro-elastic plates *J. Intell. Mater. Syst. Struct.* **30** 1757–71
[79] Vinyas M, Harursampath D and Nguyen-Thoi T 2020 Influence of active constrained layer damping on the coupled vibration response of functionally graded magneto-electro-elastic plates with skewed edges *Defence Technology* (https://doi.org/10.1016/j.dt.2019.11.016)
[80] Hassanzadeh-Aghdam M K, Mahmoodi M J and Ansari R 2016 Interphase effects on the thermo-mechanical properties of three-phase composites *Proc. Inst. Mech. Eng. Part C J. Mech. Eng. Sci.* **230** 3361–71
[81] Dinzart F and Sabar H 2011 Magneto-electro-elastic coated inclusion problem and its application to magnetic-piezoelectric composite materials *Int. J. Solids Struct.* **48** 2393–401
[82] Vinyas M, Sunny K K, Harursampath D, Nguyen-Thoi T and Loja M A R 2019 Influence of interphase on the multi-physics coupled frequency of three-phase smart magneto-electro-elastic composite plates *Compos. Struct.* **226** 111254
[83] Haghgoo M, Hassanzadeh-Aghdam M K and Ansari R 2018 Effect of piezoelectric interphase on the effective magneto-electro-elastic properties of three-phase smart composites: a micromechanical study *Mech. Adv. Mater. Struct.* **0** 1–16
[84] Haghgoo M, Ansari R, Hassanzadeh-Aghdam M K and Darvizeh A 2019 Fully coupled thermo-magneto-electro-elastic properties of unidirectional smart composites with a piezoelectric interphase *Proc. Inst. Mech. Eng. Part C J. Mech. Eng. Sci.* **233** 2813–29
[85] Baz A and Ro J 1995 Optimum design and control of active constrained layer damping *J. Vib. Acoust.* **117(B)** 135–44